TITLE

The balance between antiviral and antibacterial responses during *M. Tuberculosis* infection is regulated by the ubiquitin ligase CBL

Authors:

Tina Truong[1,2], Kelsey Martin[1], Michelle Salemi[3], Abigail Ray[1,4], Brett S. Phinney[3], Bennett H. Penn[1,5]*

Affiliations:

1 Department of Internal Medicine, University of California, Davis, Davis, California, United States of America

2 Graduate Group in Immunology, University of California, Davis, Davis, California, United States of America

3 Proteomics Core Facility, University of California, Davis, Davis, California, United States of America

4 Microbiology Graduate Group, University of California, Davis, Davis, California, United States of America

5 Department of Medical Microbiology and Immunology, University of California, Davis, Davis, California, United States of America

*Corresponding author

ABSTRACT

As a first line of immune defense, macrophages must be able to appropriately sense and respond to diverse types of pathogens. In addition, many pathogens activate multiple sensors and

generate complex signals in a responding cell. How macrophages integrate multiple pathogen-associated signals into a coherent physiologic response is unclear. Upon entering a macrophage, *M. tuberculosis* (*Mtb*) induces proinflammatory cytokines that activate antibacterial responses. Surprisingly, it also triggers antiviral responses that actually hinder the host response to *Mtb*. The ubiquitin ligase CBL suppresses these antiviral responses and shifts macrophages toward a more antibacterial state during *Mtb* infection. However, the mechanisms by which CBL regulates immune signaling are unknown. We found that CBL broadly suppresses the expression of antiviral effector genes and then used quantitative mass-spectrometry to identify potential CBL substrates. We identified over 46,000 ubiquitylated sites in *Mtb*-infected macrophages, and subsequent analysis of CBL-deficient cells identified roughly 400 CBL-dependent ubiquitylation events, highlighting potential substrates. Using genetic interaction analysis of CBL and its putative substrates we identified the Fas associated factor 2 (FAF2) adapter protein as a key signaling molecule protein downstream of CBL. Together, these analyses identify thousands of new ubiquitin-mediated signaling events during the innate immune response and reveal an important new regulatory hub in this response.

INTRODUCTION

Being among the first cells to respond to infection, tissue macrophages must be able to sense and effectively respond to diverse types of pathogens, ranging from multicellular eukaryotic parasites to bacteria and viruses. Longstanding clinical observations have suggested potential antagonism between types of immune responses targeting different classes of microbe. Patients with preceding influenza virus infection carry roughly a 100-fold higher near-term risk of developing bacterial pneumonia from *Streptococcus pneumoniae* (1). Similarly, while CD4 T helper 2 (Th2) cells are critical for responses to multicellular parasites, patients with Th2-dominant immune responses in *Mycobacterium leprae* lesions harbor higher bacterial loads and experience more severe disease (2).

Even in the simple scenario of a single immune cell encountering a lone pathogen, the mechanisms by which the type of pathogen is discerned, and an appropriate response mounted remains poorly understood. Dozens of individual sensors for diverse bacterial-, fungal-, and virus-associated PAMPS have been described (3,4). However, most pathogens activate multiple sensors simultaneously, and how these multiple signals are integrated into a coherent pathogen-appropriate immune response remains unclear.

Mycobacterium tuberculosis (*Mtb*) persists as a threat to human health. It currently infects one-third of the world's population, causing a chronic, often lifelong infection, and tuberculosis (TB) kills an estimated 1-2 million people annually (5). Macrophages infected with *Mtb* are immediately exposed to an array of cell wall-derived pathogen-associated molecular patterns (PAMPs) such as lipoarabinomannan, lipoproteins, and peptidoglycan which activate cognate receptors such as TLR2, NOD2 and CLEC4E (Mincle) (6–14). The outcome of many of these signaling pathways is the activation of nuclear factor kappa B (NFκB) family transcription factors and the upregulation of proinflammatory cytokines such as TNF and IL1B which activate potent antibacterial responses and are critical for controlling *Mtb* replication (15–22).

Surprisingly, *Mtb* also activates numerous antiviral effectors in infected macrophages. *Mtb* rapidly permeabilizes its phagosome and releases bacterial nucleic acids into the host cytosol through unclear mechanisms (24–26). Bacterial DNA is recognized by cyclic GMP-AMP synthase (cGAS) which then triggers STING-dependent activation of IRF3 and IRF7 transcription factors, causing upregulation of hundreds of genes, including the type I interferons like interferon beta (IFN-β) that propagate the signal to nearby cells (24,25,27–31). Bacterial RNA is also introduced into the host cell, initiating signaling through the retinoic acid-Inducible gene I (RIG-I) sensor which triggers MAVS-dependent activation of IRF3/IRF7with similar effects (25). While these initial observations came from mouse models, gene expression analysis of TB patients has detected similar activation of type I IFN in the peripheral blood of patients with active TB (32–34).

74 Several lines of evidence demonstrate that these antiviral responses interfere with the
75 antibacterial capacity of macrophages, and suggest that macrophages can be polarized into
76 antiviral or antibacterial states by their encounter with a pathogen. C3H-derived strains of mice
77 harbor a polymorphism causing loss of the SP140 transcriptional repressor, resulting in
78 hyperactivation IFN-β. These strains are highly susceptible to *Mtb*, succumbing rapidly with
79 dramatically increased bacterial burdens (35–39) – a phenotype that is rescued by the
80 administration of an IFN-β blocking antibody or by loss of the type I interferon receptor (IFNAR)
81 (39,40). B6 mice infected with *Mtb* produce lower levels of IFN-β following infection, but even in
82 this context, loss of MAVS or IFNAR results in decreased bacterial burden and increased survival
83 of infected animals (25,26) Thus, activation of antiviral responses within the host seems to actively
84 interfere with an effective antibacterial response to *Mtb*, and suggests that *Mtb* might introduce
85 nucleic acids into the host cell as a virulence strategy,

86 Ubiquitin signaling plays an important role in regulating both antibacterial and antiviral
87 responses in *Mtb*-infected macrophages. Ubiquitin ligases such as PARKIN and SMURF are
88 critical for targeting *Mtb* for autophagy (41–44). Separately, the ubiquitin ligases TRIM14 and CBL
89 have been shown to regulate the expression of type I interferon following *Mtb* infection (45,46).
90 CBL is targeted by the secreted *Mtb* virulence factor LpqN, which is required for *Mtb* replication
91 in mice. Proteomic analyses identified a physical interaction between LpqN and CBL, and the
92 growth of the attenuated *lpqN Mtb* mutant was rescued by disruption of host *Cbl* (45). While *Cbl*-
93 deficient macrophages are more permissive for *Mtb* replication, the opposite is seen with viral
94 challenge, as CBL-deficient macrophages more potently restrict viral replication (45). Together,
95 these findings suggest that CBL is an important regulator of antiviral versus antibacterial
96 polarization of macrophages. However, how CBL regulates this process are not known.

97 Here, we investigated the mechanisms by which CBL regulates immune signaling. We
98 found that it controls macrophage responses to multiple stimuli and represses the expression of

99 numerous antiviral effectors. We then used proteomics to identify potential CBL substrates in
100 macrophages as they respond to *Mtb* infection and identified the endoplasmic reticulum-localized
101 signaling adapter Fas-associated factor 2 (FAF2) as a protein that undergoes CBL-dependent
102 ubiquitylation. Notably, while CBL deficient macrophages are more permissive for *Mtb* growth,
103 simultaneous loss of FAF2 in double-knockout macrophages reverses this phenotype, suggesting
104 that the FAF2 pathway might be hijacked by *Mtb,* and that CBL acts to constrain FAF2 activity in
105 *Mtb*-infected macrophages.

106 **RESULTS**

107 **CBL broadly suppresses antiviral effector expression.**

108 Prior work has shown that CBL suppressed host antiviral responses in mouse primary
109 bone-marrow-derived macrophages (BMDMs) following *Mtb* infection (45). We began by
110 assessing whether this role of CBL was evolutionarily conserved, with CBL also regulating these
111 processes in human cells. We used shRNA to deplete CBL mRNA in the human THP-1 cell line
112 that differentiates into macrophage-like cells after stimulation with Phorbol-12-myristate-13-
113 acetate (PMA) and 1,25-dihydroxy-Vitamin D. We first assessed whether loss of CBL in human
114 macrophages would similarly rescue the growth of the CBL-sensitive *lpqN*::Tn mutant *Mtb* strain
115 (hereafter *lpqN* mutant) which lacks the effector that normally antagonizes CBL function, and
116 which is attenuated in both mouse BMDMs and in mice (45). Following differentiation, we infected
117 THP-1 control cells expressing a non-targeting shRNA, and CBL-depleted cells expressing a
118 CBL-specific shRNA (Fig 1A). To monitor bacterial replication, we used the *lpqN* mutant carrying
119 a bioluminescent *LuxBCADE* reporter operon (45), and then monitored bacterial growth by
120 quantifying bacterial luminescence over time. Consistent with prior observations in mouse
121 BMDMs, we found that loss of CBL also rescued the growth of the *lpqN* mutant in human
122 macrophages. (Fig 1B). The increased bacterial replication was confirmed by direct colony
123 forming unit (CFU) numeration (Fig S1A) and was associated with a more rapid loss of

124 macrophage viability in CBL-deficient macrophages over the course of infection (Fig 1C). The
125 effect of CBL on *Mtb* replication was independently confirmed using a second independent shRNA
126 in THP-1 cells (Fig S1B). To confirm these findings, we evaluated the role of CBL in a second
127 human macrophage line, HL-60. We used shRNA to deplete CBL (Fig 1D) and found that loss of
128 CBL similarly rescued the growth of *lpqN* mutant *Mtb* in these cells as well (Fig 1E).

Fig 1. CBL suppresses antiviral responses in human cells. (A) CBL expression analyzed by RT-qPCR analysis of THP-1 cells expressing CBL-specific shRNA and control non-targeting shRNA (B) Luminescent growth assay of CBL-sensitive *lpqN Mtb* mutant expressing *LuxBCADE* operon. (C) Phase-contrast microscopy images of infected macrophages prior to and 96 h post-infection (MOI=0.8, 10x magnification; scale bar 100μm). (D) RT-qPCR analysis of CBL expression in HL-60 cells. (E) Luminescent growth assay of *lpqN Mtb* in HL-60 cells. (F),(G) RT-qPCR analysis of *lpqN*-infected macrophages 6 h after infection. Analysis of (H) THP-1 or (I) HL60 cells transfected with either RNA or DNA as indicated. Means ± SEM are displayed. MOI= 0.8 for THP-1 growth assays, 1.0 for HL-60 growth assays, and MOI=10 for RNA analyses. Data is representative (median) of three or more independent experiments. Statistical significance testing by t-test indicated on plot, p-value: * ≤0.05, **≤0.01, ***≤0.001, ns >0.05.

129 We next determined whether antiviral gene expression was also regulated by CBL in
130 human cells. Consistent with prior observations in mouse macrophages, we found that depletion
131 of CBL resulted in an increased expression of antiviral effectors was increased in THP-1 and HL-
132 60 cells following *Mtb* infection (Fig 1F,G). We next used defined PAMPs to selectively stimulate
133 different pathways leading to IFN-β activation to assess if CBL was regulating a single pathway
134 or multiple pathways. Work from several groups has shown that *Mtb* activates IFN-β both through
135 the cGAS DNA sensing pathway as well as the RIG-I RNA sensing pathway (24-25,31-32). To
136 assess which pathways are regulated by CBL, we individually transfected THP-1 and HL-60

137 macrophages with either dsDNA, a known agonist for cGAS, or with 5′-phosphorylated RNA, a
138 known agonist for RIG-I, in order to evaluate the role of CBL. We found that in response to either
139 DNA or 5' phosphorylated RNA, loss of CBL resulted in an increased expression of IFN-β in THP-
140 1 cells (Fig 1H). In HL-60 cells we observed a similar role for CBL in regulating RNA-stimulated
141 IFN-β responses. However, following DNA stimulation HL-60 cells displayed only weak induction
142 of IFN-β, and did so independently of CBL (Fig 1I). Taken together these data support a model
143 where the role of CBL in innate immunity is evolutionarily conserved, acting to suppress
144 expression of antiviral effectors such as IFN-β in multiple different contexts.

145 We next sought to determine whether CBL selectively regulated a restricted group of
146 genes, such as IFIT1 and IFN-β, or whether it orchestrated broad transcriptional changes in
147 macrophages as they responded to *Mtb*. To assess this, we infected THP-1 cells with *Mtb*, using
148 the *lpqN* mutant strain so that CBL activity would be unconstrained by the bacterial effector. We
149 infected both control and CBL-deficient THP-1 cells for 6 h, when many immune-related genes
150 are strongly induced, and prepared RNA for expression profiling by RNA-Seq. As expected, *Mtb*
151 infection of control cells triggered widespread gene expression changes with upregulation of 735
152 genes and downregulation of 423 genes (FDR ≤0.05, Log2 fold-change > 0.5) and strong
153 induction of both proinflammatory and antiviral effectors. (Fig S2A, Table S1). CBL-deficient cells
154 regulated most of these same genes in a similar manner following *Mtb* infection. However, one
155 set of genes showed distinct CBL-dependent transcriptional changes, with 204 genes
156 hyperactivated and 62 genes depressed in CBL-deficient cells following *Mtb* infection (Fig 2A and
157 Table S1). Interestingly, while CBL regulates the production of IFN-β in these cells (Fig 1G, 1I) it
158 does not regulate the response of cells to IFN-β stimulation (Fig S2B), suggesting that the broad
159 CBL-dependent gene expression changes are due to cell-intrinsic mechanisms and not the
160 indirect effects of type I interferon.

161

Fig 2. CBL regulates a complex transcriptional program. (A) RNA-Seq differential gene expression analysis of THP-1 macrophages expressing CBL-specific shRNA vs control non-targeting shRNA 6 h after infection with *lpqN*-mutant *Mtb.* (B) Biological processes transcriptionally regulated by CBL. (C), (D) Differential expression of immune response genes in CBL-deficient cells. (E) ENCODE Transcription factor binding site enrichment of CBL-regulated genes (F) RT-qPCR analysis of CBL-regulated genes after indicated stimuli. Differentially-expressed genes for analyses in (B-E) defined by RNA-Seq FDR<0.05 and Log2 fold-change>0.5.

162 We further analyzed the set of genes regulated by CBL to evaluate what cellular processes
163 were being affected, and what transcription factors might be mediating the regulatory effects of
164 CBL. We performed systematic pathway enrichment analysis using the Gene Ontology and
165 KEGG Databases and identified several clusters of functionally-related genes regulated by CBL.
166 Supporting the hypothesis that CBL broadly suppresses antiviral responses, we found a
167 significant over-representation of antiviral defense genes in the set of CBL-regulated genes (10-
168 fold over-representation, FDR <0.02). We also found significant associations with several other
169 pathways including IL-10 production and global protein translation (Fig 2B-D).

170 In addition, we analyzed the set of genes transcriptionally regulated by CBL to determine
171 whether any associations existed between these genes and characterized transcriptional
172 regulators. We assessed this by systematically querying the ENCODE Chip-Seq database (47)
173 with the set of genes regulated by CBL. In uninfected cells, there were no transcriptional
174 regulators enriched at these genes. In contrast, in *Mtb*-infected cells, analysis of the 266 CBL-
175 responsive genes using ENCODE showed an association with several transcriptional regulators
176 (Fig 2E). The most significant association was seen with for the NFkB family member RELA, with
177 an odds-ratio (OR) of 2.6 p 1≤E-9) found at a set of immune-related genes, with additional

178 associations noted for STAT2 (OR=5.3, p≤2E-7), ATF1 (OR=2.5, p≤1.1E-8), and MYC (OR=2.1,
179 p≤5E-8, Fig 2E).

180 We also assessed whether genes we identified as regulated by CBL during *Mtb* infection
181 were also regulated by CBL in response to other stimuli. We selected TLR8 and CXCL10, two
182 genes identified by our RNA-Seq analysis of *Mtb*-infected macrophages whose expression was
183 suppressed by CBL and examined their regulation in cells exposed other PAMPs - either
184 cytoplasmic dsDNA to activate cGAS or 5'-phosphorylated RNA to activate RIG-I. In both cases
185 we found hyperactivation of these genes in CBL-deficient cells, although the patterns differed
186 somewhat. For TLR8 we detected basal de-repression in unstimulated cells and hyperactivation
187 following Mtb infection and either DNA or RNA stimulation. For CXCL10, there was no basal de-
188 repression, and while CXCL10 was strongly regulated by CBL during *Mtb* infection, it showed only
189 modest increases in expression in CBL-deficient cells stimulated with DNA or RNA (Fig 2F). Taken
190 together, these results demonstrate that CBL regulates a broad subset of antiviral response genes
191 in macrophages, along with regulation of several other processes, and that it does so in response
192 to multiple stimuli, perhaps by regulating events upstream of RELA or STAT2.

193 **CBL enzymatic activity is required to regulate macrophage responses to Mtb**

194 We next sought to determine the mechanisms by which CBL regulates immune responses.
195 CBL is a RING-domain E3 ligase that was initially characterized as a proto-oncogene,
196 ubiquitylating activated receptor tyrosine kinases to target them for degradation (48–50).
197 Subsequent studies using an enzymatically inactive CBL point mutant showed that CBL also has
198 important non-enzymatic functions, and can act as a signaling scaffold that potentiates
199 phosphatidylinositol 3-kinase and SRC-family kinase activity (51). This non-enzymatic function
200 plays an important role in vivo, as several of the developmental defects *Cbl*$^{-/-}$ mice could be
201 rescued by expression of enzymatically-inactive CBL (52).

202 To test whether CBL was acting enzymatically to ubiquitylate key substrates during innate
203 immune responses, or whether it was acting as a signaling adapter protein, we performed genetic
204 complementation analysis in CBL-deficient macrophages, re-introducing either wild type CBL or
205 catalytically inactive mutants. To study human macrophages, we used shRNA-expressing CBL-
206 deficient THP-1 cells. For mouse cells, we used Cas9-expressing conditionally-immortalized
207 macrophages (CIMs) expressing an sgRNA targeting *Cbl* (hereafter *Cbl*$^{-/-}$). CIM cells carry a
208 HOXB8-ER estrogen-regulatable transcription factor that maintains the cells as immortalized
209 monocyte precursors in the presence of estrogen, but upon estrogen withdrawal allows
210 differentiation into macrophages closely recapitulating the physiology of primary mouse BMDMs
211 (53). For both mouse and human cells, we used lentiviral vectors to deliver either catalytically
212 inactive CBL (human C381A, mouse C379A) or WT CBL (Fig 3A). In both cases, CBL expression
213 was restored to ~50% of endogenous levels, without evidence of destabilization of the mutant
214 protein (Fig 3B). As seen previously (45), CBL-deficient macrophages were more permissive for
215 *Mtb* replication than control cells, and as expected, in both mouse and human macrophages, re-
216 introduction of WT CBL significantly restricted the growth of *Mtb* (Fig 3C,D). In contrast, re-
217 introduction of catalytically-inactive CBL failed to complement the defective host response,
218 demonstrating that enzymatic activity is needed for CBL function in this context. Interestingly, cells
219 expressing inactive CBL actually had higher bacterial loads than CBL-deficient cells, suggesting
220 that catalytically-inactive CBL might act as a dominant-negative isoform, perhaps by interfering
221 with the activity of other signaling molecules such as the related CBL-family ligase CBLB.

222 **Identifying potential CBL substrates**

223 Given that the enzymatic activity of CBL was necessary to regulate immune signaling, we
224 next sought to identify CBL substrates in this context. Several growth factor receptors including
225 EGFR, and CSF1R have been characterized as CBL substrates in other settings (48–50).
226 However, the CBL substrates during innate immune responses are not known. We used *Cbl*$^{-/-}$ CIM

227 cells to study ubiquitylation because of the near-complete loss of CBL protein in the polyclonal
228 population of cells expressing a CBL-specific sgRNA, and their larger *Mtb* growth phenotype
229 relative to human cells partially depleted of CBL via shRNA (Fig 3B-D). Using the *lpqN* mutant
230 strain that is unable to antagonize CBL activity, we infected cells for 6 h, and added the
231 proteasome inhibitor bortezomib for the final 2 h to stabilize ubiquitylated proteins and facilitate
232 their detection by mass-spectrometry (MS).

Fig 3. CBL-dependent ubiquitylation is required to restrict *Mtb* growth in mouse and human macrophages. (A) CBL domain structure and catalytic site mutants. (B) Immunoblot of wild-type and mutant CBL protein re-introduced into CBL-deficient human (THP-1) and mouse (CIM) macrophages. (C), (D) Luminescent growth assay of *lpqN Mtb* in CBL-deficient macrophages in which CBL expression was restored with either wild-type or mutant CBL. (E) Experimental design for ubiquitylation proteomics using di-Gly MS. (F) diGly-MS analysis of ubiquitylation in control CIM cells expressing a non-targeting sgRNA 6 h after infection with the *lpqN Mtb* mutant. Green (increased) and blue (decreased) indicate peptides with p-val ≤0.01 and Log2 fold-change >2. (G) Comparison of ubiquitylation versus total-protein changes in control cells following infection. Green (increased) and blue (decreased) denote data points where the change in di-Gly peptide abundance was >3 standard-deviations greater than the change in protein abundance. (H) Subset of CBL-dependent changes (I) diGly-MS analysis of ubiquitylation 6 h post-infection in control vs. *Cbl*$^{-/-}$ cells infected with *lpqN Mtb*. (J) Ubiquitylation versus total-protein changes in control vs. *Cbl*$^{-/-}$ cells (K) Biological process of proteins with CBL-dependent ubiquitylation. Cells were infected at MOI=0.8 for growth assays and MOI=10 for diGly-MS. Di-gly MS was analysis of 3 independent experiments. Growth assays are representative (median) of at 3 or more replicates.

233 We then used di-Gly enrichment MS to globally monitor changes in ubiquitylation in *Mtb*-
234 infected cells. Lysates were prepared from uninfected and infected cells, and from control and

235 *Cbl*$^{-/-}$ cells, and digested with trypsin. We then enriched ubiquitylated peptides by
236 immunoprecipitation with an antibody that recognizes the di-Gly remnant of ubiquitin that remains
237 conjugated to the ubiquitin-modified Lys residue following trypsinization and analyzed the
238 samples by liquid chromatography tandem MS (LC-MS/MS), using label-free quantification (Fig
239 3E and Ref. 54–59). Of note, the ubiquitin-like proteins ISG15 and NEDD8 leave an
240 indistinguishable di-Gly-Lys remnant. However, these modifications account for only ~5% of
241 identified di-Gly modified residues, and the vast majority of di-Gly sites are ubiquitin-modified (60–
242 62). In addition, since CBL is a ubiquitin-specific ligase, any CBL-dependent di-Gly modifications
243 should represent CBL-dependent ubiquitylation. Thus, we will hereafter refer to di-Gly-modified
244 sites as ubiquitylation, recognizing that a small percentage of non-CBL-dependent sites are
245 modified by ISG15 or NEDD8.

246 Overall, we identified ~76,000 unique peptides in macrophages, encompassing ~46,000
247 unique di-Gly-modified sites. This dataset creates the most detailed atlas of ubiquitin modification
248 in macrophages to date, with roughly 10-fold more sites identified than currently available
249 datasets of this specialized cell type. As expected, in control cells, we saw numerous ubiquitin
250 changes in response to *Mtb* with a total of 1,793 ubiquitylation sites increasing (Log2 fold-change
251 >1, FDR <0.05) and 197 sites decreasing (Fig 3F, Table S2). Since the quantity of a ubiquitylated
252 peptide in a sample can change because of either a change in the stoichiometry of ubiquitylation
253 at a given site, or because of a change in abundance of the protein itself, we sought to
254 deconvolute these processes. We examined changes in protein abundance in the same samples
255 by quantitative LC-MS/MS (Table S3) and analyzed the change in ubiquitylation at each site
256 relative to the change in protein expression. This analysis demonstrated a range of stoichiometry
257 changes. For proteins such as RSAD2 and IL1B, the increased quantity of ubiquitylated peptides
258 was largely due to increased protein expression (Fig 3G). Conversely, proteins like IKBKE and
259 GABARAP had large changes in ubiquitylation stoichiometry with minimal change in overall

260 protein levels. Overall, changes in abundance of a ubiquitylated peptide and protein abundance
261 were poorly correlated (R^2=0.36) and in roughly 70% of cases the changes in stoichiometry was
262 3 standard-deviations greater than protein abundance (Fig 3H) indicating that in a majority of
263 cases the change in abundance of a ubiquitylated peptide was independent of protein abundance
264 and due to a change in the stoichiometry of ubiquitylation.

265 We next examined ubiquitylation in CBL-deficient macrophages following *Mtb* infection.
266 As expected, the loss of CBL did not change the abundance of most ubiquitylated peptides,
267 consistent with a complex ubiquitin signaling landscape involving numerous E3 ligases. However,
268 there was also a clear subset of peptides that underwent CBL-dependent ubiquitylation, including
269 well-established CBL substrates such as the receptor tyrosine kinases MET and CSFR1. As
270 anticipated, most changes seen in *Cbl*$^{-/-}$ cells were peptides with decreased ubiquitylation; there
271 were 430 ubiquitylation sites that decreased (Log2FC >1.0, FDR<0.05) and 90 sites increased in
272 abundance (Fig 3I). Changes in the stoichiometry of ubiquitylation drove the changes in
273 abundance of the di-Gly peptides, with very little correlation between changes in abundance for
274 ubiquitylated peptides and protein expression (R^2=0.09, Fig 3J).

275 Systematic analysis of the proteins with CBL-dependent ubiquitylation demonstrated the
276 enrichment of several pathways and processes; several had clear immune-related functions such
277 as regulation of phagocytosis (7.1-fold over-representation, p≤0.01), vacuolar acidification (13.7-
278 fold, p=0.02), NFkB regulation (7.2-fold, p=0.02), and IFNGR signaling (4.2-fold, p≤0.01). There
279 were also factors known to be involved in the immune response to *Legionella pneumophila* (5.3-
280 fold, p≤0.01), *Salmonella enterica* (3.2-fold , p ≤0.001, and *Mtb* itself (3.1- fold, p<0.01). Several
281 other unanticipated pathways were also over-represented in the set of proteins with CBL-
282 dependent ubiquitylation, including endoplasmic reticulum-associated protein degradation
283 (ERAD) pathway (6.2-fold-fold over-representation, p≤0.001) and iron uptake (6.1-fold, p≤1E-4).
284 Taken together, these findings suggest that the set of proteins ubiquitylated by CBL extends far

285 beyond its established role in growth-factor signaling at the plasma membrane and includes
286 several other cellular processes throughout the cytoplasm and on membrane-bound organelles.

287 **Function of proteins with CBL-dependent ubiquitylation**

288 We next sought to identify which proteins with CBL-dependent ubiquitylation played
289 important roles during *Mtb* infection. We identified a subset of 43 proteins that had peptides with
290 at least 80% reduction in ubiquitylation in *Cbl*$^{-/-}$ cells. Of these, 20 had annotated functions
291 associated in some way with innate immunity (Fig 4A), and we analyzed this set of 20 proteins
292 for CBL-dependent functions during *Mtb* infection. We hypothesized that if a protein is an
293 important substrate of CBL, then loss of that protein should either phenocopy the CBL mutant (if
294 positively regulated by CBL) or reverse the CBL phenotype (if inhibited by CBL). To analyze each
295 of these factors we designed a lentiviral vector with two sgRNA cassettes, thereby allowing us to
296 generate mutant CIM cell lines lacking either CBL or a putative CBL substrate, as well as double-
297 mutant cells lacking both simultaneously (Fig 4B). Editing efficiency of >80% was confirmed by
298 either TIDE analysis of genomic DNA (85), or by immunoblot of the targeted protein (Fig 4C).
299

Fig 4. FAF2 promotes *Mtb* replication in the absence of CBL. (A) Examples of changes in ubiquitylation and total protein for immune regulators in *Mtb*-infected *Cbl*$^{-/-}$ CIM cells 6 h post-infection. (B) Experimental design for creation of cells lacking both *Cbl* and putative substrates. (C) Immunoblot of FAF2 protein in CIM cells expressing either non-targeting or *Faf2*-specific sgRNA. (D) Luminescent growth assay of *lpqN*-mutant *Mtb*. (E) Location of ubiquitylated residues on FAF2 and Log2 fold-change of ubiquitylation at each residue site in *Mtb*-infected *Cbl*$^{-/-}$ cells vs. control cells. (F) Immunoblot of FAF2 protein levels in *Mtb*-infected control and *Cbl*$^{-/-}$ cells. Representative data of four independent experiments are shown. Error bars represent SEM.

300 We then infected each of these mutant cell lines with the CBL-sensitive *lpqN Mtb* mutant
301 and assessed bacterial growth. As expected, the growth of *Mtb* was more rapid in CBL-deficient
302 cells (Fig 4D), and in most cases, loss of a putative substrate in these CBL-deficient cells did not
303 alter the replication of *Mtb* (data not shown). However, disruption of the Fas-associated factor 2
304 (*Faf2*) locus in CBL-deficient cells significantly altered the antibacterial capacity of these cells
305 toward *Mtb*. FAF2 is an ER-localized signaling adapter protein, and our di-Gly MS analysis found
306 it to be heavily ubiquitylated in macrophages, with 9 different ubiquitylated Lys residues. In *Cbl*$^{-/-}$
307 cells, a single residue (K246) showed a specific loss of ubiquitylation, with other Lys residues
308 relatively unaffected (Fig 4E). In contrast to the other genes tested, disruption of FAF2 in CBL-
309 deficient cells restored the ability of these cells to restrict *Mtb* replication, with bacterial growth
310 rates approaching that seen in control macrophages that received a non-targeting sgRNA.

311 Given the established role of CBL in targeting cell-surface receptors for degradation, we
312 tested the idea that CBL similarly targets FAF2 for degradation through ubiquitylation. However,
313 FAF2 protein levels did not change following Mtb infection and were unaltered in CBL-deficient
314 macrophages (Fig 4F). This suggests that rather than regulating FAF2 levels, CBL-dependent
315 ubiquitylation is instead regulating the function of FAF2, perhaps by altering its protein-protein
316 interactions. Taken together, these genetic analyses show that while multiple proteins undergo
317 CBL-dependent ubiquitylation, FAF2 seems to be an important regulatory hub downstream of
318 CBL as macrophages respond to *Mtb* infection.

319 **DISCUSSION**

320 **Immune response polarization**

321 Macrophages must be able to sense and effectively respond to diverse types of
322 pathogens. Both clinical data and animal models indicate that while a particular type of immune
323 response may be beneficial in some circumstances, it can be detrimental in others. Tissue
324 macrophages act as first responders in many infections, acting both to clear pathogens and to

325 direct subsequent immune responses. However, how a macrophage determines the type of
326 pathogen it is encountering and translates that into an appropriate response remains unclear.

327 *Mtb* exposes an infected macrophage to an array of PAMPS; some are distinctively
328 bacterially-derived molecules such as peptidoglycan or lipoarabinomannan, which activate NOD2
329 and TLR2 respectively. Activation of these sensors results in the release of cytokines with potent
330 antibacterial activities such as TNF and IL1B (5–8,10,11). However, *Mtb*, as well as a number of
331 other intracellular bacterial pathogens, including *Listeria monocytogenes,* and *Chlamydia*
332 *trachomatis,* also activate cytosolic nucleic-acid sensors such as cGAS and induce expression of
333 type I interferon and other antiviral effectors (63–66). While type I interferon potently inhibits
334 viruses and can inhibit the growth of some bacteria such as *C. trachomatis*, it impairs antibacterial
335 responses to *Mtb* and *L. monocytogenes* in mice (63–66).

336 The observation that antiviral responses can actively antagonize the antibacterial capacity
337 of a macrophage suggests that macrophages might become polarized into antibacterial versus
338 antiviral states. It also suggests that pathogens infecting macrophages like *Mtb,* and *L.*
339 *monocytogenes* might seek to subvert this process as a virulence strategy. In the case of *Mtb*, it
340 seems to do so through several mechanisms. First, upon perforation of its phagosome, *Mtb*
341 exposes bacterial dsDNA to the host cell cytoplasm which initiates a cascading activation of
342 cGAS, STING, TBK1, and IRF3. IRF3 then triggers a complex transcriptional program, inducing
343 the expression of IFN-β, as well as hundreds of other downstream genes, many of which have
344 potent antiviral activity (24–31). Second, in parallel, *Mtb* also releases bacterial RNA into the host
345 cytosol, thereby activating a similar RIG-I, MAVS, TBK1, and IRF3 pathway resulting in IFN-β
346 expression (25). *Mtb* also introduces the LpqN virulence factor into host cells which interferes with
347 the ability of the CBL ubiquitin ligase to regulate this process, thereby amplifying antiviral
348 responses (45).

349 Exactly how the expression of antiviral effectors such as IFN-β antagonizes the
350 antibacterial state of a macrophage is unclear. Integrating the results of different studies that
351 examined different viral response regulators suggests that the transcriptional program controlling
352 the expression of antiviral proteins such as IFN-β is likely to be comprised of several distinct
353 modules, as the perturbation of different regulators causes distinct *Mtb*-related phenotypes. For
354 example, in isolated ex vivo macrophages, disruption of CBL, TRIM14, or IRF7 alters the
355 expression of antiviral effectors and alters the ability of a macrophage to restrict *Mtb* replication
356 (45,46,67). In contrast, perturbation of RIG-I, SP140 or IFNAR has no effect on *Mtb* replication in
357 isolated macrophages but profoundly alters *Mtb* susceptibility in mice (25,39,40,67–70). This
358 suggests that while all these pathways regulate IFN-β signaling, they might differ in their
359 regulation of other target genes, and that these differences drive distinct physiologic states in *Mtb*-
360 infected macrophages. It also suggests that the additional regulatory inputs impinging on an
361 infected macrophage during a complex immune response in vivo create a distinct environment
362 where type I interferon signaling becomes a dominant factor.

363 **CBL Substrates**

364 Although the mechanisms by which CBL regulates growth factor signaling are known in
365 detail, the mechanisms by which it regulates innate immunity are not. CBL was initially
366 characterized as a proto-oncogene that ubiquitylates activated receptor tyrosine kinases, thus
367 targeting them for degradation, and was later found to have non-enzymatic functions in activating
368 phosphatidylinositol 3-kinase and SRC-family kinases (48,49,51,71). We found that the enzymatic
369 activity of CBL was needed for its ability to regulate immune responses during *Mtb* infection and
370 identified the signaling adapter protein FAF2 as a critical intermediary factor, disruption of FAF2
371 rescued the impaired responses in CBL-deficient cells. This suggests a scenario where FAF2
372 might somehow be hijacked by *Mtb* to impair host defenses, and that CBL normally acts to
373 constrain FAF2 activity in *Mtb*-infected macrophages.

374 FAF2 is known to regulate a diverse set of physiologic processes, and thus the manner
375 by which FAF2 regulates the innate immune response to *Mtb* is uncertain. FAF2 was originally
376 characterized as a member of a family of ubiquitin regulatory X (UBX) domain proteins regulating
377 the endoplasmic-reticulum-associated degradation pathway (ERAD) (72). FAF2 was also
378 subsequently shown to act as a positive regulator of STING, MTOR, and NFκB activation (73–
379 75). Which of these pathways is the critical one downstream of FAF2 during *Mtb* infection is an
380 important remaining question.

381 It is also unclear what function the CBL-dependent ubiquitylation of FAF2 at K246 plays.
382 A straightforward explanation would have been that CBL inhibits FAF2 by targeting it for
383 degradation, analogous to the regulation of growth-factor receptors (49,76,77). However, our data
384 demonstrate that this is not the case. Instead, it seems that ubiquitylation alters FAF2 functionality,
385 perhaps by modulating its interactions with STING, MTOR, or NFκB or their regulators. Future
386 genetic experiments analyzing FAF2 alleles with mutations in K246 should provide insight into the
387 function of FAF2 ubiquitylation, as will biochemical experiments analyzing the activation state of
388 these different pathways.

389 **Ubiquitylation during *Mtb* infection**

390 These studies also create a detailed atlas of protein ubiquitylation in macrophages as they
391 respond to a pathogen, generating intriguing new hypotheses about how ubiquitin signaling might
392 regulate innate immunity. Although numerous proteomics studies have analyzed ubiquitylation in
393 mammalian cells, few of these focused on immune cells, and only a handful have examined
394 signaling during innate immune responses to pathogens. Such studies in activated immune cells
395 have provided important insights by identifying specific ubiquitylation events contributing to
396 autophagy and DNA repair processes during infection that alter immune responses (78,79). Here,
397 we identified ~46,000 unique di-Gly-modified Lys residues, significantly broadening the scope of
398 the ubiquitin-mediated signaling events taking place in macrophages as they respond to a

399 pathogen. These analyses reveal a number of previously unknown ubiquitylation events on critical
400 immune regulators, including the secreted cytokines IL1A and TNFSF13B, the endosomal
401 peptidoglycan transporter SLC15A3, and the cytoplasmic peptidoglycan sensor NOD2 (Table S2).
402 Thus, this dataset suggests multiple new mechanisms by which ubiquitin signaling might be
403 regulating other critical immune responses.

404 **Limitations**

405 While our RNA-Seq data show clear CBL-dependent transcriptional changes in CBL-
406 depleted THP-1 macrophages, this is an imperfect model system. The expression of CBL is only
407 reduced ~85% by shRNA, and it is possible that residual CBL activity could be masking some
408 changes. Although we also used CRISPR/Cas9 genome-editing to generate *CBL*$^{-/-}$ THP-1 clones,
409 we observed marked clone-to-clone variability in *Mtb*-related phenotypes. In addition, the
410 response of cell lines such as THP-1 cells to immune stimuli is often muted relative to primary
411 macrophages (53). For example, we note that while changes in IFN-β expression were readily
412 detectible in *Mtb*-infected THP-1 cells by RT-qPCR, the overall transcript levels were too low for
413 reliable quantification by RNA-Seq. Separately, our MS studies had some limitations. They
414 identified a large number of peptides with the di-Gly-Lys remnant, and while ~95% of di-Gly
415 modifications result from ubiquitylation, NEDD8 and ISG15 both leave identical di-Gly remnants.
416 Our current data are unable to distinguish the small subset of Lys residues modified by these
417 other ubiquitin-related proteins. However, since CBL is believed to be a ubiquitin-specific ligase
418 the set of CBL-dependent changes are likely due to ubiquitin. Finally, for those proteins with CBL-
419 dependent ubiquitylation, we cannot distinguish at this time between direct ubiquitylation by CBL
420 versus indirect effects of CBL mediated by another E3 ligase or deubiquitinase that it regulates.

421

422 **SUPPLEMENTAL FIG LEGENDS**

423 **Fig S1.** (A) CFU determination in THP-1 cells expressing either CBL-specific or non-targeting
424 control shRNA 5d after infection with *lpqN Mtb.* (B) Luminescent growth assay of *lpqN Mtb* in a
425 secondary independent CBL shRNA in THP-1 cells.

426 **Fig S2.** (A) RNA-seq analysis of control THP-1 cells expressing a non-targeting shRNA,
427 comparing uninfected and *lpqN Mtb*-infected cells. (B) RT-qPCR analysis of IFIT1 in IFN-β
428 stimulated THP-1 cells.

429

430 **MATERIALS AND METHODS**

431 **Key Reagent Table**

REAGENT OR RESOURCE	SOURCE	IDENTIFIER
Antibodies		
Rabbit c-CBL antibody	Cell Signaling Technology	Cat # 2747
β-Actin (C4) Alexa Fluor® 680	Santa Cruz Biotechnology	Cat # sc-47778 AF680
PTMScan® Ubiquitin Remnant Motif (K-ε-GG)	Cell Signaling Technology	Cat # 5562S
FAF2 antibody	Proteintech	Cat # 16251-1-AP
IRDye® 800CW Donkey anti-Mouse IgG Secondary Antibody	Li-cor	Cat # 926-32212
IRDye® 800CW Goat anti-Rabbit IgG Secondary Antibody	Li-cor	Cat # 926-32211
Primer and guide sequences		
qPCR_*IFNβ* Human F	This paper	CTTCTCCACTACAGCTCTTTCC

qPCR_*IFNβ* Human R	This paper	GCCAGGAGGTTCTCAACAATA
qPCR_*IFIT1* Human F	This paper	CCAGAAATAGACTGTGAGGAAGG
qPCR_*IFIT1* Human R	This paper	CCCTATCTGGTGATGCAGTAAG
qPCR_*β-ACTIN* Human F	This paper	GACCACCTTCAACTCCATCAT
qPCR_*β-ACTIN* Human R	This paper	CCTGCTTGCTAATCCACATCT
ms_*Actin*_qpcr_FW	This paper	GGTGTGATGGTGGGAATGG
ms_*Actin*_qpcr_RV	This paper	GCCCTCGTCACCCACATAGGA
ms_*Ifnβ*_qPCR_FW	This paper	TCCGAGCAGAGATCTTCAGGAA
ms_*Ifnβ*_qPCR_RV	This paper	TGCAACCACCACTCATTCTGAG
ms_*Ifit1*_qPCR_FW	This paper	CGTAGCCTATCGCCAAGATTTA
ms_*Ifit1*_qPCR_RV	This paper	AGCTTTAGGGCAAGGAGAAC
		AGTTACGCGTCTCTAAACCCATG
		TTCCAGTTATGCTGCGGGAAAGAGTGGTCT
Lg_m*Faf2*gRNA_Rv	This paper	CATACAG
Lg_m*Faf2*geno_Fw	This paper	CTAGTAGTTACAGTGTGCTTGC
Lg_m*Faf2*geno_Rv	This paper	CTGTGAACATTTCTGTTGCTCC
		GAAGTCTGCTAACATGCGGTGACG
		TCGAGGAGAATCCTGGCCCAATGGCCAAG
T2A_BSF_F	This paper	CCTTTGTCTCAAG

		GACGTCACCGCATGTTAGCAGACTTCCCCTG
Strep_T2A_R	This paper	CCCTCGCCGGAGCCGGGCCCCTTCTCGAACTGGGGGTGGCTCCAG
Bla_R_	This paper	CTTTGTACAAGAAAGCTGGGTCTAGATTTAGCCCTCCCACACATAACCAGAGGGC
Bacterial strains		
CDC1551 *lpqN*:Tnhimar1 mutant	BEI Resources	Cat # NR-18454
Cell lines		
THP-1	ATCC	TIB-202
HL-60	ATCC	CCL-240
HOXB8-ER Rosa26Cas9 CIM	Gift from Greg Barton, UC Berkeley	N/A
B16	ATCC	CRL-6475
3T3-MCSF	Gift from Russell Vance, UC Berkeley	

Chemicals

Middlebrook OADC	Thermo Fisher Scientific	Cat # b12351
BD DIFCO™ Middlebrook 7H9	Becton Dickinson (BD)	Cat # 271310
BD DIFCO™ Middlebrook 7H10	Becton Dickinson (BD)	Cat # 262710
PTMScan Lys-C Protease	Cell Signaling Technology	Cat # 39003
Sequencing Grade Modified Trypsin	Promega	Cat # V5111
Bortezomib	Cell Signaling Technology	Cat # 2204S
cOmplete™, Mini, EDTA-free Protease Inhibitor Cocktail	Sigma Aldrich	Cat # 11836170001
Bovine growth serum	Hycolone	SH30541.03
Fetal bovine serum	Corning	5-015-CV

Phorbol 12-myristate 13 acetate (PMA)	Sigma Aldrich	Cat # P8139
1α,25-Dihydroxyvitamin D3 (Vitamin D)	Santa Cruz	Cat # 32222-06-3
SYBR™ Gold Nucleic Acid Gel Stain	Invitrogen	Cat # S11494
Poly(ethylene glycol) 8000	Sigma	Cat # 81268
Lipofectamine 2000	Invitrogen	Cat # 11668030

Consumables

500mg Sep-Pak C18 columns	Waters	Cat # WAT036790
PureLink™ RNA Mini Kit	Invitrogen	Cat # 12183018A
Maxima H Minus Reverse Transcriptase	Thermo Scientific	Cat # EP0753
0.45 µm Acrodisc Syringe Filters	Pall	Cat # 4614

Recombinant DNA

lentiGuide Puro	Addgene	Plasmid #52963
pENTR1a	Thermo	A10462
pLenti CMV blast DEST	Addgene	Plasmid #17451

pLenti CMV no selection marker	This paper	
pLKO.1 puro	Addgene	Plasmid #8453

Software and websites

Prism v9.0	GraphPad	
Rstudio	Posit	
Synthego guide design tool	Synthego	https://design.synthego.com
TIDE analysis		https://tide.nki.nl/

Other

Odyssey CLx	Li-Cor	
Glomax Explorer	Promega	
CFX Connect Real-Time System	BIO-RAD	
Whole-body exposure chamber 099C A4212	Glas-Col	

Deposited data

At the time of publication raw MS data files will be deposited at MasIVE https://massive.ucsd.edu/ProteoSAFe. RNA-Seq data will be deposited at GEO https://www.ncbi.nlm.nih.gov /geo/info/seq.html. Processed MS and RNA-Seq data will be available as supplementary data files at the time of publication.

438 **Cell Lines**

439 THP-1 human monocytes (ATCC TIB-202) and HL-60 promyeloblast cells (ATCC CCL-240) were
440 purchased from ATCC. THP-1 cells were cultured in RPMI media containing 10% fetal bovine
441 serum (FBS), 10mM HEPES, 1mM sodium pyruvate, 4500 mg/L glucose, and 0.05 mM 2-
442 mercaptoethanol. HL-60 cells are cultured in RPMI containing 10% bovine growth serum (BGS),
443 15% fetal bovine serum (FBS), 1mM sodium pyruvate, 2mM L-glutamine, and 1X MEM non-
444 essential amino acids solution. HOXB8-ER and Cas9-expressing conditionally immortalized
445 macrophages (CIMs) were cultured in RPMI media containing 10% FBS, 10mM HEPES, 1mM
446 sodium pyruvate, 2mM L-glutamine, 1.5ul 2-mercaptoethanol, 2% GM-CSF as conditioned media
447 from B16 cells murine melanoma cells, and 2uM β-estradiol as previously described (53), prior to
448 differentiation. THP-1 and HL-60 cells were differentiated with DMEM supplemented with 10%
449 FBS, 1mM pyruvate, 2mM L-glutamine, 10ng/ml phorbol 12-myristate 13 acetate (PMA), and
450 0.1ng/ml 1,25 dihydroxy-vitamin D. Cells were differentiated for 72 h before experiments. CIM
451 cells were differentiated by washing to removal of β-estradiol and then culture with DMEM
452 supplemented with 10% FBS, 2mM L-glutamine, 1mM sodium pyruvate, 10% MCSF (derived
453 from 3T3 MCSF conditioned media) for 7 days prior to experiments.

454 All cell lines generated using lentiviral vectors followed the same steps of transfection of
455 HEK 293T Lenti-X cells with the transfer vector expressing the gene of interest, alongside the
456 packaging plasmids psPAX2 and the envelope plasmid VSV-G. Viral supernatant is harvested 48
457 hours after transfection and either filtered with a 0.45 µm syringe filter and for CIM cell
458 transduction, concentrated using A PEG-8000 solution (80). For transduction, viral supernatant
459 with Polybrene 8ug/ml is added for 12h to THP-1 and HL-60 cells. CIM cells are transduced
460 through spinfection and spun for 2h at 1000 RPM at 32C and then incubated for 6h before washing
461 and culture in fresh media. Selective antibiotics were as follows: THP-1 and HL-60 cells are

462 selected with 0.5 μg/ml of Puromycin or 4 μg/ml of Blasticidin. CIM cells are selected with 8 μg/ml
463 of Puromycin or 4 μg/ml of Blasticidin.

464 **Bacterial Strains**

465 *Mtb* was cultured in 7H9 (BD) supplemented with 0.5% glycerol, 10% oleic acid-albumin-dextrose-
466 catalase (OADC, Middlebrook), and 0.1% Tween-80 in bottles gently rotated at 40 RPM at 37° C
467 or on 7H10 plates supplemented with 10% OADC, 0.5% glycerol, and 0.1% Tween 80 at 37° C.

468 **Macrophage Infection for RNA harvest:**

469 *Mtb* strains were prepared for inoculation by washing twice in PBS with 10% heat-inactivated
470 horse serum, gently sonicated, and spun at 500 rpm for 5 m to generate a fine bacterial
471 suspension. Bacteria were opsonized in 10% heat-inactivated horse serum and macrophages
472 were infected at an MOI = 10 for 6hr by spinfection at 1200RPM for 10 minutes followed by
473 washing in PBS. After incubation, wells are washed once with 1X PBS and harvested in Trizol for
474 RNA extraction.

475 **Macrophage Infection for Lux assay:**

476 For luminescent growth assays, cells are plated in triplicate in 96 well plates at a density of 8 x
477 10^4 cells/well for THP-1 cells and 1.5 x 10^5 cells/ well for CIM cells. Macrophage cell density at
478 the time of infection was carefully matched between control and experimental cell lines to within
479 <15% variance by plating sets of control wells across a gradient of densities and using SYBR gold
480 to quantify nucleic acid content of plated experimental and control cells. Macrophages are infected
481 at a MO1 = 0.8, and after spinfection plates are incubated for 30 minutes at 37° C. After the
482 incubation, the monolayers were washed with PBS containing 1% heat-inactivated horse serum
483 twice, and bacterial luminescence was measured over time in a GloMax Explorer warmed to 37
484 degrees C. Macrophage growth media was changed every other day. Colony-forming units
485 (CFUs) were quantified by lysing triplicate wells of macrophages in sterile water and plated in

486 serially dilutions on 7H10 agar with supplemented with OADC and 0.1% Tween-80. Plates were
487 incubated at 37° C for 3 weeks prior to CFU enumeration.

488 **Western Blots**

489 Protein in cell lysates was quantified by BCA. 30-50ug of protein lysate was separated by SDS-
490 PAGE and transferred onto nitrocellulose membranes and blocked with LiCor blocking buffer at
491 0.5x for 1h. Primary antibodies were used at varying dilutions and incubated 1.5h at room-
492 temperature or, in the case of anti-CBL antibody, 4° C overnight. Secondary antibodies were used
493 at 1:10,000 dilution for 1h. After probing for indicated antibodies, the membranes were imaged on
494 an Odyssey scanner (Licor).

495 **RNA Purification**

496 Nucleic acid-stimulated macrophages were lysed in PureLink lysis buffer per manufacturer
497 instructions. *Mtb*- infected macrophages were lysed in Trizol. In both cases, lysates were purified
498 with silica spin columns (Purelink) per manufacturer instructions.

499 **Macrophage nucleic acid stimulation and RT-qPCR**

500 Differentiated THP-1 and HL-60 cells are plated at 8 x 10^5/ well in a 12-well plate. Cells are
501 stimulated with 10ng of RNA or 20ng of DNA delivered by Lipofectamine 2000 as per manufacturer
502 instructions and incubated for 6h. After RNA purification, cDNA was generated using 500ng total
503 RNA with Maxima H minus reverse transcriptase and diluted 1:10 before qPCR analysis with the
504 indicated primers and SYBR Green I detection of products.

505 **RNA-seq**

506 Differentiated THP-1 cells were infected at MOI=10 for 6 h with *lpqN Mtb* in three independent
507 experiments on different days. RNA was purified and barcoded 3'Tag-Seq libraries prepared using
508 the QuantSeq FWD kit (Lexogen, Vienna, Austria) for multiplexed sequencing according to the
509 recommendations of the manufacturer by the UC Davis DNA Sequencing core. The fragment size

510 distribution of the libraries was verified via micro-capillary gel electrophoresis on a Bioanalyzer
511 2100 (Agilent, Santa Clara, CA). The libraries were quantified by fluorometry on a Qubit
512 instrument (Life Technologies, Carlsbad, CA), and pooled in equimolar ratios. Twelve libraries
513 were sequenced on one lane of an Aviti sequencer (Element Biosciences, San Diego, CA) with
514 single-end 100 bp reads. The sequencing generated more than 4 million reads per library.
515 Analysis of human data: HTStream was used to remove PhiX, adapter sequences, polyA tails,
516 low quality sequences from end of reads, N bases, and reads less than 50 basepairs. After
517 preprocessing, STAR was used to align reads to GRCh38.p13 human genome. UMI-tools was
518 used to remove PCR duplicates post-alignment. Next, feature Counts was use to count reads
519 whose alignment overlapped with genes using the gencode genome corresponding to the human
520 genome version used. Annotation used was version 41. R was used for limma-voom pipeline on
521 R with multiple testing correction using Benjamini-Hochberg procedure.

522 **Plasmid Construction for short shRNA and sgRNA delivery**

523 shRNA expression plasmids were constructed by digesting pLKO.1 cloning vector with AgeI and
524 EcoRI and annealed oligonucleotides containing the 21 shRNA encoding sequence were inserted,

525 **For sgRNA,** 20 nucleotide targeting sequences were designed to target regions in the first exon
526 of each locus using the Synthgo design tool. The targeting sequence is then fused by overlap-
527 extension PCR to a second-generation tracRNA (81) and inserted into the HpaI and XhoI sites of
528 pSicoR . The dual-guide sgRNA vector was constructed using a synthesized gene block
529 containing the two guides of interest and an H1 promoter from Integrated DNA technologies (IDT)
530 that were digested with BsmBI v2 on both ends and ligated to BsmBI v2 digested Lentiguide Puro
531 vector (Addgene) with a second-generation tracRNA (81). Evaluation of editing efficiency was
532 performed using TIDE.

533 CRISPR/Cas9 genome editing.

534 After lentiviral delivery of sgRNA cells were selected for 1 week with puromycin. The genome
535 editing efficiency of the polyclonal population evaluated by PCR amplification of the targeted exon
536 followed by Sanger sequencing and TIDE analysis. The polyclonal population was used for
537 experiments

538 **Site-directed mutagenesis**

539 The wildtype and ligase mutant copies of CBL for both THP-1 and CIM cells contain synonymous
540 mutations at the targeting sites of either the RNAi or CAS9 system to prevent degradation. Site-
541 directed mutagenesis was carried out to generate catalytically inactive CBL mutants using
542 pENTR1a plasmids (Addgene). Mutagenesis was validated through Sanger sequencing.
543 Following validation, gateway cloning was used to move the mutated CBL open reading frame
544 from pENTR1a into lentiviral pDEST vectors (Addgene). For THP-1 cells, constructs were cloned
545 into a pLenti CMV Blast vector (Addgene). For CIM cells, constructs were fused by overlap
546 extension PCR directly to a T2A peptide and blasticidin resistance gene and were cloned into
547 pLenti CMV modified to remove other antibiotic resistance genes (82).

548 **Ubiquitination Proteomics**

549 3 x 10^7 cells were plated 24h before infection. Cells were infected with *lpqN Mtb* at an MOI = 10
550 for 6 hours. 2h prior to harvest, the 1μM of Bortezomib is added. For harvest, cells were washed
551 1X with PBS then scraped in ice-cold methanol+ 0.1 glycine pH 2.5 to precipitate protein, and
552 inactivate proteases and *Mtb.* Cells were scrapped and removed from the BSL3. Chloroform was
553 added to 20% volume to assist precipitation, incubated on ice for 10 min. and samples centrifuged
554 to pellet protein. The pellets were washed once with ice-cold methanol, recentrifuged, and dried.
555 Protein was resolubilized in in 9M Urea 25 mM HEPES pH 8.5,1 mM chloroacetamide (CAM),
556 0.5x Complete-mini protease inhibitor, and 0.5 mM EDTA with sonication. Proteins were then
557 reduced for 45 min with 5 mM dithiothreitol (DTT) at room temperature and alkylated with 20mM
558 CAM for 20 minutes at room temperature and in the dark. BCA assay was performed, samples

559 diluted 1:4 in HEPES pH 8.0 and 2.5 mg of protein digested with Lys-C at enzyme to substrate
560 ratio 1:100 at 37°C for 2h. Subsequently, samples were digested overnight at 37°C with trypsin
561 enzyme to substrate ratio 1ug:100ug. Digestion was stopped with 0.5% TFA and then incubated
562 on ice for 15 min to allow urea to precipitate and samples centrifuged to pellet debris. Peptides
563 were desalted with 500 mg Sep-Pal C18 columns as per manufacturer instructions and
564 lyophilized.

565 **Immunoprecipitation of di-Gly-containing peptides**

566 2.5mg of lyophilized peptides were resuspended with 0.5x immunoaffinity purification (IAP) buffer
567 (50mM MOPS, pH7.2; 10mM sodium phosphate; 50mM NaCl) and sonicated. 10 ul cross-linked
568 anti-K-ε-GG antibody beads were washed 3x in PBS. Samples were then mixed with 10 ul cross-
569 linked anti-K-ε-GG antibody beads and incubated at 4°C for 2h. The peptide-bead mixture was
570 then washed four times with PBS and one time with 0.1x IAP. Peptides were eluted with 100ul
571 0.15% TFA and analyzed by LC-MS/MS with on-tip clean up prior to MS run.

572 **Mass-Spectrometry**

573 Chromatography was performed on an Evosep 1 using either the 60spd (di-Gly) or 30spd
574 (total protein) method. Each sample was loaded onto a disposable Evotip C18 trap column
575 (Evosep Biosytems, Denmark) as per the manufacturer's instructions. Briefly, Evotips were wetted
576 with 2-propanol, equilibrated with 0.1% formic acid, and then samples were loaded using
577 centrifugal force at 1200g. Evotips were subsequently washed with 0.1% formic acid, and then
578 200 µL of 0.1% formic acid was added to each tip to prevent drying. The tipped samples were
579 subjected to nanoLC on a Evosep One instrument (Evosep Biosystems). Tips were eluted directly
580 onto a PepSep analytical column, dimensions: 150umx10cm C18 column (PepSep, Denmark)
581 with 1.5 µm particle size (100 Å pores) (Bruker Daltronics), and a ZDV spray emitter (Bruker
582 Daltronics). Mobile phases A and B were 100% water with 0.1% formic acid (v/v) and 100%

583 Acetonitrile 0.1% formic acid (v/v), respectively. The standard pre-set method of 30 samples-per-
584 day was used, which is a 44 min minute run or 60 spd which is a 21 min run.

585 Mass Spectrometry – Performed on a hybrid trapped ion mobility spectrometry-quadrupole
586 time of flight mass spectrometer (timsTOF Pro 2 and timsTOF HT, (Bruker Daltonics, Bremen,
587 Germany) with a modified nano-electrospray ion source (CaptiveSpray, Bruker Daltonics). In the
588 experiments described here, the mass spectrometer was operated in diaPASEF mode.
589 Desolvated ions entered the vacuum region through the glass capillary and deflected into the
590 TIMS tunnel which is electrically separated into two parts (dual TIMS). Here, the first region is
591 operated as an ion accumulation trap that primarily stores all ions entering the mass spectrometer,
592 while the second part performs trapped ion mobility analysis.

593 DIA PASEF: The dual TIMS analyzer was operated at a fixed duty cycle close to 100%
594 using equal accumulation and ramp times of 75 ms each. For the 30spd Evosep run, Data-
595 independent analysis (DIA) scheme consisted of one MS scan followed by MSMS scans taken
596 with 6x3= 18 precursor windows at width of 50Th per 6x3= 560 ms cycle, over the mass range
597 8x3= 300-1200 Dalton. The TIMS scans layer the doubly and triply charged peptides over an ion
598 mobility -1/k0- range of 0.707-1.29 V*sec/cm2. The collision energy was ramped linearly as a
599 function of the mobility from 59 eV at 1/K0=1.2 to 20 eV at 1/K0=0.7. For the 60spd Evosep run,
600 Data-independent analysis (DIA) scheme consisted of one MS scan followed by MS/MS scans
601 taken with 5x7= 35 precursor windows at width of 30^{Th} = 763 ms cycle time over the mass range
602 286-1307 Dalton. The TIMS scans layer the doubly and triply charged peptides over an ion
603 mobility -1/k0- range of 0.7-1.3 V*sec/cm2. The collision energy was ramped linearly as a function
604 of the mobility from 59 eV at 1/K0=1.2 to 20 eV at 1/K0=0.

605 **Data Analysis**

606 LCMS files were processed with Spectronaut version 18.4(Biognosys, Zurich, Switzerland) using
607 DirectDIA analysis mode. Mass tolerance/accuracy for precursor and fragment identification was

608 set to default settings. The unreviewed FASTA for Mus Musculus, UP000000589, downloaded
609 from Uniprot and a universal library of common laboratory contaminants (Frankenfield et al, 2022).
610 For di-Gly analysis, a maximum of two missing cleavages were allowed, the required minimum
611 peptide sequence length was 7 amino acids, and the peptide mass was limited to a maximum of
612 4600 Da. Carbamidomethylation of cysteine residues was set as a fixed modification, and
613 methionine oxidation, acetylation of protein N termini and ubiquitination as variable modifications.
614 A decoy false discovery rate (FDR) at less than 1% for peptide spectrum matches and protein
615 group identifications was used for spectra filtering (Spectronaut default). Decoy database hits,
616 proteins identified as potential contaminants, and proteins identified exclusively by one site
617 modification were excluded from further analysis. For total protein: DIA data was analyzed using
618 Spectronaut 18. using the direct DIA workflow with PTM localization selected. Trypsin/P Specific
619 was set for the enzyme allowing two missed cleavages. Fixed Modifications were set for
620 Carbamidomethyl, and variable modifications were set to Acetyl (Protein N-term), Oxidation, and
621 ubiquitination. For DIA search identification, PSM and Protein Group FDR were set at 0.01%.
622 Mass-spectrometry statistical analysis was performed in Spectronaut® (Biognosys) using t-test
623 with multiple testing correction.

624 **Pathway enrichment analysis**

625 Functional and pathway enrichment analysis for RNAseq Ubiquitination Proteomics

626 Gene ontology and pathway analysis were carried out on the set of genes with FDR <= 0.5 and
627 LogFC <= 0.5 using the DAVID database (Database for Annotation, Visualization and Integrated
628 Discovery; https://david.ncifcrf.gov/) (84). The significantly enriched biological pathways were
629 identified with FDR <0.05. The pathways were visualized using R.

630 **Statistics**

631 Statistical significance for RT-qPCR data was performed using GraphPad Prism version 10
632 (GraphPad Software, LLC) using two-tailed Student t-test when comparing. Statistical analysis
633 for RNA-sequencing datasets was performed using the limma-voom pipeline on R with multiple
634 testing corrections using Benjamini-Hochberg procedure. Ubiquitination statistical analysis was
635 carried out within Spectronaut® (Biognosys) using the integrated statistical package with
636 randomized imputation of values near the limit of detection if a peptide was undetectable in a
637 particular sample, and performs t-tests with multiple testing correction and FDR calculation.

638 **Acknowledgements**

639 We would like to thank Sebastian Winter and Jeroen Saeij for their input on this manuscript. We
640 would like to thank the DNA Technologies and Bioinformatics cores at UC Davis that assisted with
641 the sequencing and processing of the RNA-seq analysis. BHP was funded by NIH 1R01AI144149.

642

643 References

644 1. Shrestha S, Foxman B, Weinberger DM, Steiner C, Viboud C, Rohani P. Identifying the
645 interaction between influenza and pneumococcal pneumonia using incidence data. Sci Transl
646 Med. 2013 Jun 26;5(191):191ra84.

647 2. Yamamura M, Uyemura K, Deans RJ, Weinberg K, Rea TH, Bloom BR, et al. Defining
648 Protective Responses to Pathogens: Cytokine Profiles in Leprosy Lesions. Science. 1991 Oct
649 11;254(5029):277–9.

650 3. Mogensen TH. Pathogen Recognition and Inflammatory Signaling in Innate Immune
651 Defenses. Clin Microbiol Rev. 2009 Apr;22(2):240–73.

652 4. Li D, Wu M. Pattern recognition receptors in health and diseases. Sig Transduct Target Ther.
653 2021 Aug 4;6(1):1–24.

654 5. TB mortality [Internet]. [cited 2024 Apr 17]. Available from: https://www.who.int/teams/global-
655 tuberculosis-programme/tb-reports/global-tuberculosis-report-2023/tb-disease-burden/1-2-
656 tb-mortality

657 6. Ferwerda G, Girardin SE, Kullberg BJ, Le Bourhis L, de Jong DJ, Langenberg DML, et al.
658 NOD2 and toll-like receptors are nonredundant recognition systems of Mycobacterium
659 tuberculosis. PLoS Pathog. 2005 Nov;1(3):279–85.

660 7. Bowdish DME, Sakamoto K, Kim MJ, Kroos M, Mukhopadhyay S, Leifer CA, et al. MARCO,
661 TLR2, and CD14 are required for macrophage cytokine responses to mycobacterial trehalose
662 dimycolate and Mycobacterium tuberculosis. PLoS Pathog. 2009 Jun;5(6):e1000474.

663 8. Underhill DM, Ozinsky A, Smith KD, Aderem A. Toll-like receptor-2 mediates mycobacteria-
664 induced proinflammatory signaling in macrophages. Proc Natl Acad Sci U S A. 1999 Dec
665 7;96(25):14459–63.

666 9. Blumenthal A, Kobayashi T, Pierini LM, Banaei N, Ernst JD, Miyake K, et al. RP105 facilitates
667 macrophage activation by Mycobacterium tuberculosis lipoproteins. Cell Host Microbe. 2009
668 Jan 22;5(1):35–46.

669 10. Means TK, Wang S, Lien E, Yoshimura A, Golenbock DT, Fenton MJ. Human toll-like
670 receptors mediate cellular activation by Mycobacterium tuberculosis. J Immunol. 1999 Oct
671 1;163(7):3920–7.

672 11. Bafica A, Scanga CA, Feng CG, Leifer C, Cheever A, Sher A. TLR9 regulates Th1 responses
673 and cooperates with TLR2 in mediating optimal resistance to Mycobacterium tuberculosis. J
674 Exp Med. 2005 Dec 19;202(12):1715–24.

675 12. Dorhoi A, Nouailles G, Jörg S, Hagens K, Heinemann E, Pradl L, et al. Activation of the NLRP3
676 inflammasome by Mycobacterium tuberculosis is uncoupled from susceptibility to active
677 tuberculosis. Eur J Immunol. 2012 Feb;42(2):374–84.

678 13. Mishra BB, Rathinam VAK, Martens GW, Martinot AJ, Kornfeld H, Fitzgerald KA, et al. Nitric
679 oxide controls the immunopathology of tuberculosis by inhibiting NLRP3 inflammasome-
680 dependent processing of IL-1β. Nat Immunol. 2013 Jan;14(1):52–60.

681 14. Ishikawa E, Ishikawa T, Morita YS, Toyonaga K, Yamada H, Takeuchi O, et al. Direct
682 recognition of the mycobacterial glycolipid, trehalose dimycolate, by C-type lectin Mincle. J
683 Exp Med. 2009 Dec 21;206(13):2879–88.

684 15. Bourigault ML, Segueni N, Rose S, Court N, Vacher R, Vasseur V, et al. Relative contribution
685 of IL-1α, IL-1β and TNF to the host response to Mycobacterium tuberculosis and attenuated
686 M. bovis BCG. Immun Inflamm Dis. 2014/11/18 ed. 2013 Oct;1(1):47–62.

687 16. Segueni N, Benmerzoug S, Rose S, Gauthier A, Bourigault ML, Reverchon F, et al. Innate
688 myeloid cell TNFR1 mediates first line defence against primary Mycobacterium tuberculosis
689 infection. Scientific Reports. 2016 Mar 2;6(1):22454.

690 17. Mayer-Barber KD, Barber DL, Shenderov K, White SD, Wilson MS, Cheever A, et al. Cutting
691 Edge: Caspase-1 Independent IL-1β Production Is Critical for Host Resistance to
692 Mycobacterium tuberculosis and Does Not Require TLR Signaling In Vivo. The Journal of
693 Immunology. 2010 Apr 1;184(7):3326–30.

694 18. Pattanaik KP, Ganguli G, Naik SK, Sonawane A. *Mycobacterium tuberculosis* EsxL induces
695 TNF-α secretion through activation of TLR2 dependent MAPK and NF-κB pathways.
696 Molecular Immunology. 2021 Feb 1;130:133–41.

697 19. Mayer-Barber KD, Andrade BB, Oland SD, Amaral EP, Barber DL, Gonzales J, et al. Host-
698 directed therapy of tuberculosis based on interleukin-1 and type I interferon crosstalk. Nature.
699 2014 Jul 3;511(7507):99–103.

700 20. Di Paolo NC, Shafiani S, Day T, Papayannopoulou T, Russell DW, Iwakura Y, et al.
701 Interdependence between Interleukin-1 and Tumor Necrosis Factor Regulates TNF-
702 Dependent Control of Mycobacterium tuberculosis Infection. Immunity. 2015 Dec
703 15;43(6):1125–36.

704 21. Mayer-Barber KD, Barber DL, Shenderov K, White SD, Wilson MS, Cheever A, et al.
705 Caspase-1 independent IL-1beta production is critical for host resistance to mycobacterium
706 tuberculosis and does not require TLR signaling in vivo. J Immunol. 2010 Apr 1;184(7):3326–
707 30.

708 22. Flynn JL, Goldstein MM, Chan J, Triebold KJ, Pfeffer K, Lowenstein CJ, et al. Tumor necrosis
709 factor-α is required in the protective immune response against Mycobacterium tuberculosis in
710 mice. Immunity. 1995;2(6):561–72.

711 23. 1.2 TB mortality [Internet]. [cited 2024 Apr 17]. Available from:
712 https://www.who.int/teams/global-tuberculosis-programme/tb-reports/global-tuberculosis-
713 report-2023/tb-disease-burden/1-2-tb-mortality

714 24. Wassermann R, Gulen MF, Sala C, Perin SG, Lou Y, Rybniker J, et al. Mycobacterium
715 tuberculosis Differentially Activates cGAS- and Inflammasome-Dependent Intracellular
716 Immune Responses through ESX-1. Cell Host & Microbe. 2015 Jun 10;17(6):799–810.

717 25. Cheng Y, Schorey JS. Mycobacterium tuberculosis–induced IFN-β production requires
718 cytosolic DNA and RNA sensing pathways. J Exp Med. 2018 Nov 5;215(11):2919–35.

719 26. Stanley SA, Johndrow JE, Manzanillo P, Cox JS. The Type I IFN Response to Infection with
720 Mycobacterium tuberculosis Requires ESX-1-Mediated Secretion and Contributes to
721 Pathogenesis1. The Journal of Immunology. 2007 Mar 1;178(5):3143–52.

722 27. Creagh EM, O'Neill LAJ. TLRs, NLRs and RLRs: a trinity of pathogen sensors that co-operate
723 in innate immunity. Trends in Immunology. 2006 Aug 1;27(8):352–7.

724 28. Kawai T, Akira S. The roles of TLRs, RLRs and NLRs in pathogen recognition. Int Immunol.
725 2009 Apr;21(4):317–37.

726 29. Chen W, Han C, Xie B, Hu X, Yu Q, Shi L, et al. Induction of Siglec-G by RNA Viruses Inhibits
727 the Innate Immune Response by Promoting RIG-I Degradation. Cell. 2013 Jan
728 31;152(3):467–78.

729 30. Watson RO, Bell SL, MacDuff DA, Kimmey JM, Diner EJ, Olivas J, et al. The Cytosolic Sensor
730 cGAS Detects Mycobacterium tuberculosis DNA to Induce Type I Interferons and Activate
731 Autophagy. Cell Host & Microbe. 2015 Jun 10;17(6):811–9.

732 31. Collins AC, Cai H, Li T, Franco LH, Li XD, Nair VR, et al. Cyclic GMP-AMP Synthase Is an
733 Innate Immune DNA Sensor for Mycobacterium tuberculosis. Cell Host & Microbe. 2015 Jun
734 10;17(6):820–8.

735 32. Berry MPR, Graham CM, McNab FW, Xu Z, Bloch SAA, Oni T, et al. An interferon-inducible
736 neutrophil-driven blood transcriptional signature in human tuberculosis. Nature. 2010
737 Aug;466(7309):973–7.

738 33. Maertzdorf J, Repsilber D, Parida SK, Stanley K, Roberts T, Black G, et al. Human gene
739 expression profiles of susceptibility and resistance in tuberculosis. Genes Immun. 2011
740 Jan;12(1):15–22.

741 34. Maertzdorf J, Ota M, Repsilber D, Mollenkopf HJ, Weiner J, Hill PC, et al. Functional
742 Correlations of Pathogenesis-Driven Gene Expression Signatures in Tuberculosis. PLOS
743 ONE. 2011 Oct 28;6(10):e26938.

744 35. Moreira-Teixeira L, Tabone O, Graham CM, Singhania A, Stavropoulos E, Redford PS, et al.
745 Mouse transcriptome reveals potential signatures of protection and pathogenesis in human
746 tuberculosis. Nat Immunol. 2020 Apr 1;21(4):464–76.

747 36. Moreira-Teixeira L, Stimpson PJ, Stavropoulos E, Hadebe S, Chakravarty P, Ioannou M, et
748 al. Type I IFN exacerbates disease in tuberculosis-susceptible mice by inducing neutrophil-
749 mediated lung inflammation and NETosis. Nat Commun. 2020 Nov 4;11:5566.

750 37. Kramnik I, Dietrich WF, Demant P, Bloom BR. Genetic control of resistance to experimental
751 infection with virulent Mycobacterium tuberculosis. Proceedings of the National Academy of
752 Sciences. 2000 Jul 18;97(15):8560–5.

753 38. Kamath AB, Alt J, Debbabi H, Behar SM. Toll-Like Receptor 4-Defective C3H/HeJ Mice Are
754 Not More Susceptible than Other C3H Substrains to Infection with Mycobacterium
755 tuberculosis. Infect Immun. 2003 Jul;71(7):4112–8.

756 39. Ji DX, Yamashiro LH, Chen KJ, Mukaida N, Kramnik I, Darwin KH, et al. Type I interferon-
757 driven susceptibility to Mycobacterium tuberculosis is mediated by IL-1Ra. Nature
758 microbiology. 2019;4(12):2128–35.

759 40. Ji DX, Witt KC, Kotov DI, Margolis SR, Louie A, Chevée V, et al. Role of the transcriptional
760 regulator SP140 in resistance to bacterial infections via repression of type I interferons.
761 Stallings CL, Rath S, editors. eLife. 2021 Jun 21;10:e67290.

762 41. Franco LH, Nair VR, Scharn CR, Xavier RJ, Torrealba JR, Shiloh MU, et al. The Ubiquitin
763 Ligase Smurf1 Functions in Selective Autophagy of Mycobacterium tuberculosis and Anti-
764 tuberculous Host Defense. Cell Host Microbe. 2017 Sep 13;22(3):421–3.

765 42. Manzanillo PS, Ayres JS, Watson RO, Collins AC, Souza G, Rae CS, et al. The ubiquitin
766 ligase parkin mediates resistance to intracellular pathogens. Nature. 2013 Sep
767 26;501(7468):512–6.

768 43. Watson RO, Manzanillo PS, Cox JS. Extracellular M. tuberculosis DNA targets bacteria for
769 autophagy by activating the host DNA-sensing pathway. Cell. 2012 Aug 17;150(4):803–15.

770 44. Gutierrez MG, Master SS, Singh SB, Taylor GA, Colombo MI, Deretic V. Autophagy Is a
771 Defense Mechanism Inhibiting BCG and Mycobacterium tuberculosis Survival in Infected
772 Macrophages. Cell. 2004 Dec 17;119(6):753–66.

773 45. Penn BH, Netter Z, Johnson JR, Von Dollen J, Jang GM, Johnson T, et al. An Mtb-Human
774 Protein-Protein Interaction Map Identifies a Switch Between Host Anti-Viral and Anti-Bacterial
775 Responses. Mol Cell. 2018 Aug 16;71(4):637-648.e5.

776 46. Hoffpauir CT, Bell SL, West KO, Jing T, Wagner AR, Torres-Odio S, et al. TRIM14 Is a Key
777 Regulator of the Type I IFN Response during Mycobacterium tuberculosis Infection. J
778 Immunol. 2020 Jul 1;205(1):153–67.

779 47. Landt SG, Marinov GK, Kundaje A, Kheradpour P, Pauli F, Batzoglou S, et al. ChIP-seq
780 guidelines and practices of the ENCODE and modENCODE consortia. Genome Res. 2012
781 Sep;22(9):1813–31.

782 48. Andoniou CE, Lill NL, Thien CB, Lupher ML, Ota S, Bowtell DD, et al. The Cbl proto-oncogene
783 product negatively regulates the Src-family tyrosine kinase Fyn by enhancing its degradation.
784 Molecular and Cellular Biology. 2000;20(3):851–67.

785 49. Duan L, Miura Y, Dimri M, Majumder B, Dodge IL, Reddi AL, et al. Cbl-mediated
786 ubiquitinylation is required for lysosomal sorting of epidermal growth factor receptor but is
787 dispensable for endocytosis. Journal of Biological Chemistry. 2003;278(31):28950–60.

788 50. Andoniou CE, Thien CB, Langdon WY. The two major sites of cbl tyrosine phosphorylation in
789 abl-transformed cells select the crkL SH2 domain. Oncogene. 1996 May 2;12(9):1981–9.

790 51. Arron JR, Vologodskaia M, Wong BR, Naramura M, Kim N, Gu H, et al. A positive regulatory
791 role for Cbl family proteins in tumor necrosis factor-related activation-induced cytokine
792 (trance) and CD40L-mediated Akt activation. J Biol Chem. 2001 Aug 10;276(32):30011–7.

793 52. Thien CB, Blystad FD, Zhan Y, Lew AM, Voigt V, Andoniou CE, et al. Loss of c-Cbl RING
794 finger function results in high-intensity TCR signaling and thymic deletion. The EMBO Journal.
795 2005;24(21):3807–19.

796 53. Roberts AW, Popov LM, Mitchell G, Ching KL, Licht DJ, Golovkine G, et al. Cas9+
797 conditionally-immortalized macrophages as a tool for bacterial pathogenesis and beyond.
798 Garrett WS, Kana BD, editors. eLife. 2019 Jun 17;8:e45957.

799 54. Fulzele A, Bennett EJ. Ubiquitin diGLY proteomics as an approach to identify and quantify
800 the ubiquitin-modified proteome. Methods Mol Biol. 2018;1844:363–84.

801 55. Denis NJ, Vasilescu J, Lambert JP, Smith JC, Figeys D. Tryptic digestion of ubiquitin
802 standards reveals an improved strategy for identifying ubiquitinated proteins by mass
803 spectrometry. Proteomics. 2007 Mar;7(6):868–74.

804 56. Kim W, Bennett EJ, Huttlin EL, Guo A, Li J, Possemato A, et al. Systematic and quantitative
805 assessment of the ubiquitin-modified proteome. Mol Cell. 2011 Oct 21;44(2):325–40.

806 57. Wagner SA, Beli P, Weinert BT, Nielsen ML, Cox J, Mann M, et al. A proteome-wide,
807 quantitative survey of in vivo ubiquitylation sites reveals widespread regulatory roles. Mol Cell
808 Proteomics. 2011 Oct;10(10):M111.013284.

809 58. Xu G, Paige JS, Jaffrey SR. Global analysis of lysine ubiquitination by ubiquitin remnant
810 immunoaffinity profiling. Nat Biotechnol. 2010 Aug;28(8):868–73.

811 59. Udeshi ND, Svinkina T, Mertins P, Kuhn E, Mani DR, Qiao JW, et al. Refined preparation and
812 use of anti-diglycine remnant (K-ε-GG) antibody enables routine quantification of 10,000s of
813 ubiquitination sites in single proteomics experiments. Mol Cell Proteomics. 2013
814 Mar;12(3):825–31.

815 60. Lumpkin RJ, Gu H, Zhu Y, Leonard M, Ahmad AS, Clauser KR, et al. Site-specific
816 identification and quantitation of endogenous SUMO modifications under native conditions.
817 Nat Commun. 2017 Oct 27;8:1171.

818 61. Lobato-Gil S, Heidelberger JB, Maghames C, Bailly A, Brunello L, Rodriguez MS, et al.
819 Proteome-wide identification of NEDD8 modification sites reveals distinct proteomes for
820 canonical and atypical NEDDylation. Cell Rep. 2021 Jan 19;34(3):108635.

821 62. Zhang Y, Thery F, Wu NC, Luhmann EK, Dussurget O, Foecke M, et al. The in vivo ISGylome
822 links ISG15 to metabolic pathways and autophagy upon Listeria monocytogenes infection.
823 Nat Commun. 2019 Nov 26;10(1):5383.

824 63. He R, Torres CA, Wang Y, He C, Zhong G. Type-I Interferon Signaling Protects against
825 Chlamydia trachomatis Infection in the Female Lower Genital Tract. Infect Immun. 2023 Jun
826 15;91(6):e0015323.

827 64. Prantner D, Darville T, Nagarajan UM. Stimulator of IFN gene is critical for induction of IFN-
828 beta during Chlamydia muridarum infection. J Immunol. 2010 Mar 1;184(5):2551–60.

829 65. Leber JH, Crimmins GT, Raghavan S, Meyer-Morse NP, Cox JS, Portnoy DA. Distinct TLR-
830 and NLR-Mediated Transcriptional Responses to an Intracellular Pathogen. PLOS
831 Pathogens. 2008 Jan 11;4(1):e6.

832 66. Woodward JJ, Iavarone AT, Portnoy DA. c-di-AMP secreted by intracellular Listeria
833 monocytogenes activates a host type I interferon response. Science. 2010 Jun
834 25;328(5986):1703–5.

835 67. Johnson JR, Parry T, Repasy T, Geiger KM, Verschueren E, Budzik JM, et al. Comparative
836 analysis of macrophage post-translational modifications during intracellular bacterial
837 pathogen infection [Internet]. bioRxiv; 2020 [cited 2024 Apr 25]. p. 2020.05.27.116772.
838 Available from: https://www.biorxiv.org/content/10.1101/2020.05.27.116772v1

839 68. Bullen CK, Singh AK, Krug S, Lun S, Thakur P, Srikrishna G, et al. MDA5 RNA-sensing
840 pathway activation by Mycobacterium tuberculosis promotes innate immune subversion and
841 pathogen survival. JCI Insight. 2023 Oct 23;8(20):e166242.

842 69. Zhang L, Jiang X, Pfau D, Ling Y, Nathan CF. Type I interferon signaling mediates
843 Mycobacterium tuberculosis-induced macrophage death. J Exp Med. 2021 Feb
844 1;218(2):e20200887.

845 70. Kotov DI, Lee OV, Fattinger SA, Langner CA, Guillen JV, Peters JM, et al. Early cellular
846 mechanisms of type I interferon-driven susceptibility to tuberculosis. Cell. 2023 Dec
847 7;186(25):5536-5553.e22.

848 71. Miyake S, Lupher ML, Druker B, Band H. The tyrosine kinase regulator Cbl enhances the
849 ubiquitination and degradation of the platelet-derived growth factor receptor α. Proceedings
850 of the National Academy of Sciences. 1998;95(14):7927–32.

851 72. Christianson JC, Olzmann JA, Shaler TA, Sowa ME, Bennett EJ, Richter CM, et al. Defining
852 human ERAD networks through an integrative mapping strategy. Nat Cell Biol. 2011 Nov
853 27;14(1):93–105.

854 73. Yang L, Wang L, Ketkar H, Ma J, Yang G, Cui S, et al. UBXN3B positively regulates STING-
855 mediated antiviral immune responses. Nat Commun. 2018 Jun 13;9(1):2329.

856 74. Liu F, Tian T, Zhang Z, Xie S, Yang J, Zhu L, et al. Long non-coding RNA SNHG6 couples
857 cholesterol sensing with mTORC1 activation in hepatocellular carcinoma. Nat Metab. 2022
858 Aug;4(8):1022–40.

859 75. Gwon Y, Maxwell BA, Kolaitis RM, Zhang P, Kim HJ, Taylor JP. Ubiquitination of G3BP1
860 mediates stress granule disassembly in a context-specific manner. Science. 2021 Jun
861 25;372(6549):eabf6548.

862 76. Grøvdal LM, Stang E, Sorkin A, Madshus IH. Direct interaction of Cbl with pTyr 1045 of the
863 EGF receptor (EGFR) is required to sort the EGFR to lysosomes for degradation.
864 Experimental cell research. 2004;300(2):388–95.

865 77. Visser Smit GD, Place TL, Cole SL, Clausen KA, Vemuganti S, Zhang G, et al. Cbl Controls
866 EGFR Fate by Regulating Early Endosome Fusion. Science Signaling. 2009 Dec
867 22;2(102):ra86–ra86.

868 78. Budzik JM, Swaney DL, Jimenez-Morales D, Johnson JR, Garelis NE, Repasy T, et al.
869 Dynamic post-translational modification profiling of Mycobacterium tuberculosis-infected
870 primary macrophages. Elife. 2020 Jan 17;9:e51461.

871 79. Johnson JR, Crosby DC, Hultquist JF, Kurland AP, Adhikary P, Li D, et al. Global post-
872 translational modification profiling of HIV-1-infected cells reveals mechanisms of host cellular
873 pathway remodeling. Cell Rep. 2022 Apr 12;39(2):110690.

874 80. Torii S, Oishi W, Zhu Y, Thakali O, Malla B, Yu Z, et al. Comparison of five polyethylene glycol
875 precipitation procedures for the RT-qPCR based recovery of murine hepatitis virus,
876 bacteriophage phi6, and pepper mild mottle virus as a surrogate for SARS-CoV-2 from
877 wastewater. Science of The Total Environment. 2022 Feb 10;807:150722.

878 81. Tzelepis K, Koike-Yusa H, De Braekeleer E, Li Y, Metzakopian E, Dovey OM, et al. A CRISPR
879 Dropout Screen Identifies Genetic Vulnerabilities and Therapeutic Targets in Acute Myeloid
880 Leukemia. Cell Rep. 2016/10/21 ed. 2016 Oct 18;17(4):1193–205.

881 82. Liu Z, Chen O, Wall JBJ, Zheng M, Zhou Y, Wang L, et al. Systematic comparison of 2A
882 peptides for cloning multi-genes in a polycistronic vector. Sci Rep. 2017 May 19;7(1):2193.

883 83. Mohapatra B, Zutshi N, An W, Goetz B, Arya P, Bielecki TA, et al. An essential role of CBL
884 and CBL-B ubiquitin ligases in mammary stem cell maintenance. Development. 2017 Mar
885 15;144(6):1072–86.

886 84. Sherman BT, Hao M, Qiu J, Jiao X, Baseler MW, Lane HC, et al. DAVID: a web server for
887 functional enrichment analysis and functional annotation of gene lists (2021 update). Nucleic
888 Acids Research. 2022 Jul 5;50(W1):W216–21.

889 85. Brinkman EK, Chen T, Amendola M, van Steensel B. Easy quantitative assessment of
890 genome editing by sequence trace decomposition. Nucleic Acids Res. 2014 Dec
891 16;42(22):e168.

892

893

FIGURE 1

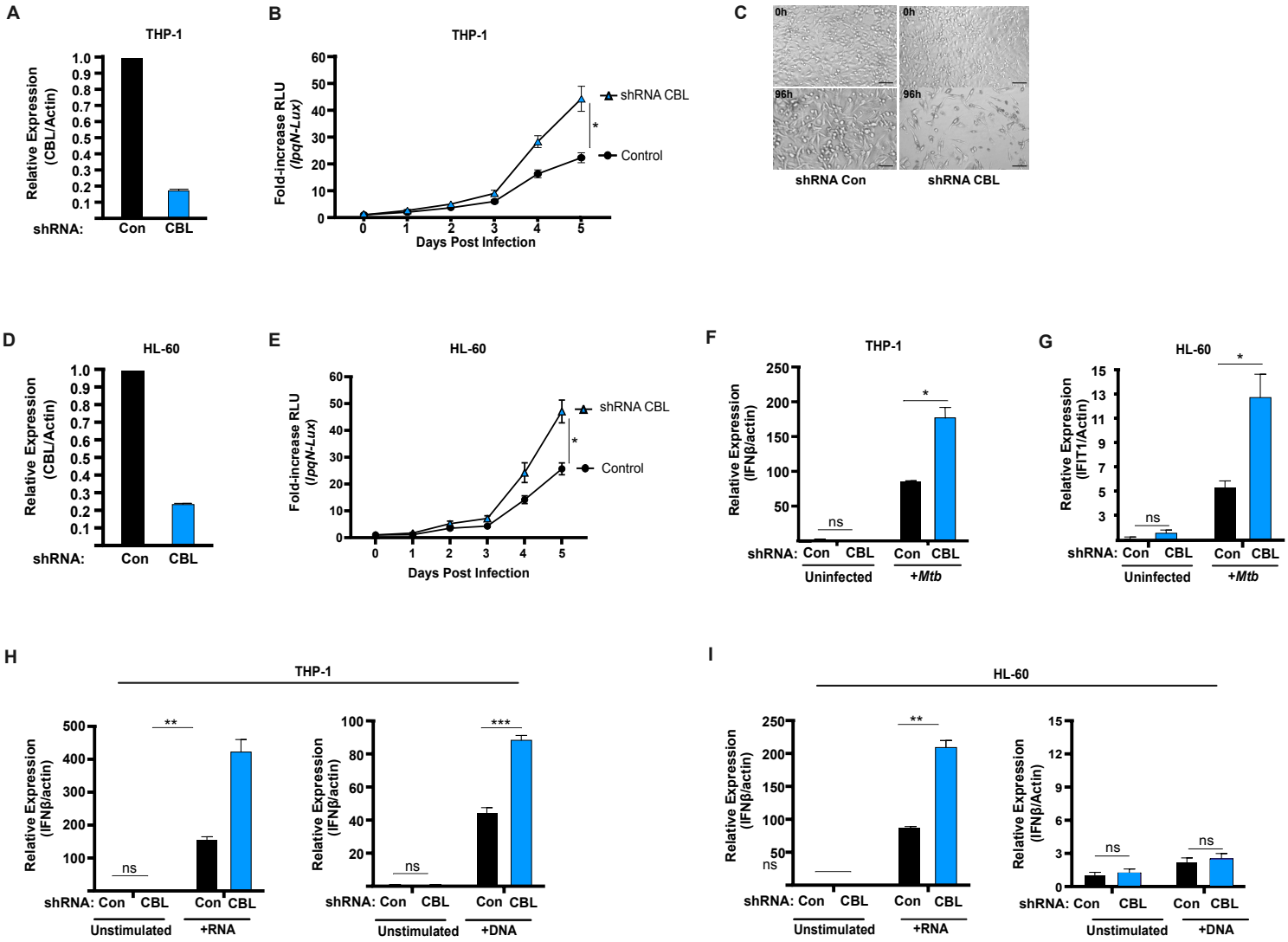
A
THP-1
Relative Expression (CBL/Actin)
shRNA: Con CBL
B
THP-1
Fold-increase RLU (lpqN-Lux)
Days Post Infection
shRNA CBL
Control
C
0h
96h
shRNA Con
shRNA CBL
D
HL-60
Relative Expression (CBL/Actin)
shRNA: Con CBL
E
HL-60
Fold-increase RLU (lpqN-Lux)
Days Post Infection
shRNA CBL
Control
F
THP-1
Relative Expression (IFNβ/actin)
shRNA: Con CBL Con CBL
Uninfected +Mtb
G
HL-60
Relative Expression (IFIT1/Actin)
shRNA: Con CBL Con CBL
Uninfected +Mtb
H
THP-1
Relative Expression (IFNβ/actin)
shRNA: Con CBL Con CBL
Unstimulated +RNA
Unstimulated +DNA
I
HL-60
Relative Expression (IFNβ/actin)
shRNA: Con CBL Con CBL
Unstimulated +RNA
Unstimulated +DNA

FIGURE 2

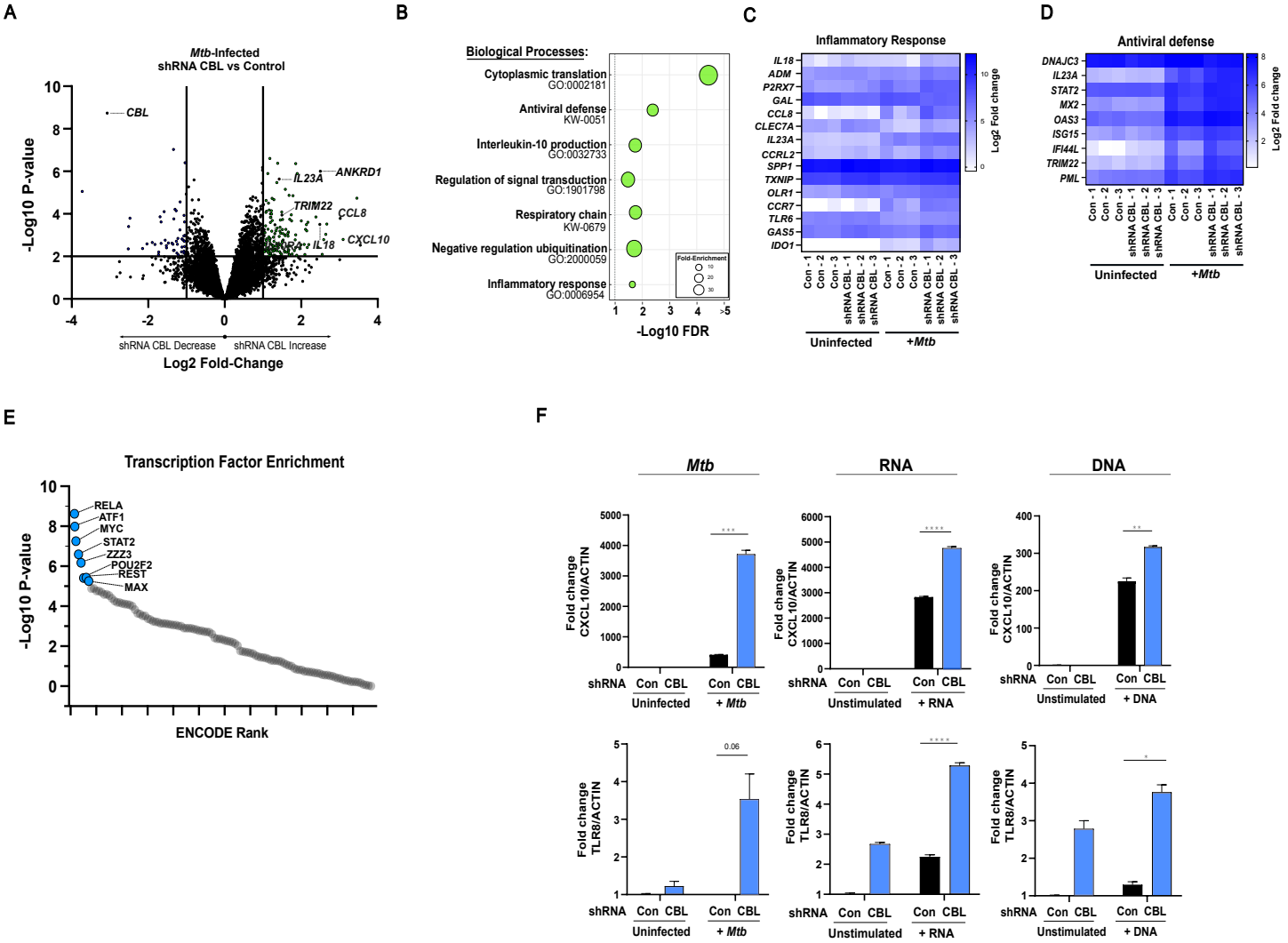
A
Mtb-Infected
shRNA CBL vs Control
-Log10 P-value
CBL
IL23A
ANKRD1
TRIM22
CCL8
IL18
CXCL10
shRNA CBL Decrease
shRNA CBL Increase
Log2 Fold-Change
B
Biological Processes:
Cytoplasmic translation
GO:0002181
Antiviral defense
KW-0051
Interleukin-10 production
GO:0032733
Regulation of signal transduction
GO:1901798
Respiratory chain
KW-0679
Negative regulation ubiquitination
GO:2000059
Inflammatory response
GO:0006954
Fold-Enrichment
-Log10 FDR
C
Inflammatory Response
IL18
ADM
P2RX7
GAL
CCL8
CLEC7A
IL23A
CCRL2
SPP1
TXNIP
OLR1
CCR7
TLR6
GAS5
IDO1
Log2 Fold change
Uninfected
+Mtb
D
Antiviral defense
DNAJC3
IL23A
STAT2
MX2
OAS3
ISG15
IFI44L
TRIM22
PML
Log2 Fold change
Uninfected
+Mtb
E
Transcription Factor Enrichment
-Log10 P-value
RELA
ATF1
MYC
STAT2
ZZZ3
POU2F2
REST
MAX
ENCODE Rank
F
Mtb
RNA
DNA
Fold change CXCL10/ACTIN
Fold change TLR8/ACTIN
shRNA
Con
CBL
Uninfected
+ Mtb
Unstimulated
+ RNA
+ DNA
0.06

FIGURE 3

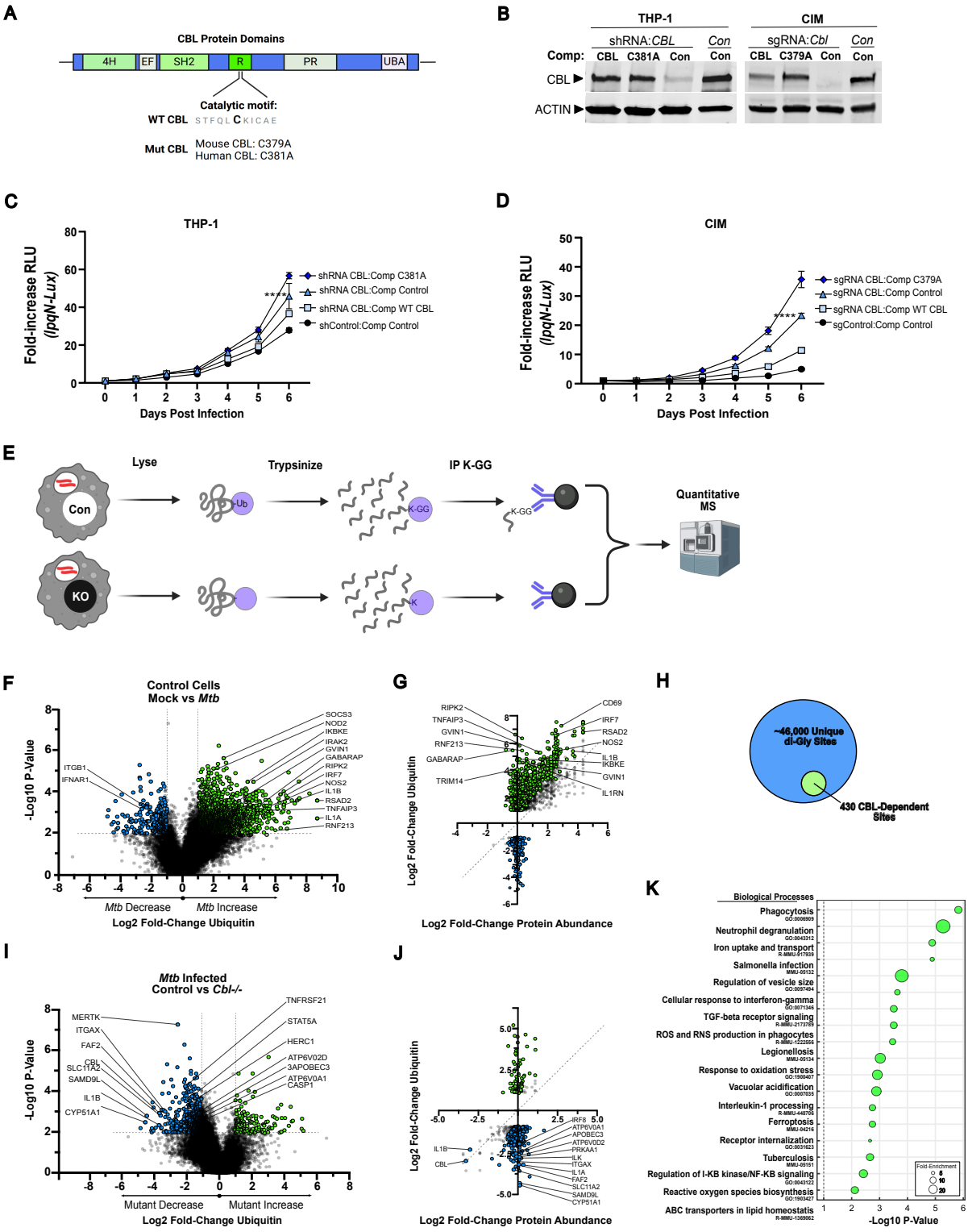
A
CBL Protein Domains
4H
EF
SH2
R
PR
UBA
Catalytic motif:
WT CBL STFQL C KICAE
Mut CBL Mouse CBL: C379A
Human CBL: C381A
B
THP-1
CIM
shRNA:CBL
Con
sgRNA:Cbl
Con
Comp: CBL C381A Con Con
CBL C379A Con Con
CBL
ACTIN
C
THP-1
Fold-increase RLU (lpqN-Lux)
Days Post Infection
shRNA CBL:Comp C381A
shRNA CBL:Comp Control
shRNA CBL:Comp WT CBL
shControl:Comp Control
D
CIM
Fold-increase RLU (lpqN-Lux)
Days Post Infection
sgRNA CBL:Comp C379A
sgRNA CBL:Comp Control
sgRNA CBL:Comp WT CBL
sgControl:Comp Control
E
Lyse
Trypsinize
IP K-GG
Quantitative MS
Con
KO
Ub
K-GG
K
F
Control Cells
Mock vs Mtb
-Log10 P-Value
Mtb Decrease
Mtb Increase
Log2 Fold-Change Ubiquitin
SOCS3
NOD2
IKBKE
IRAK2
GVIN1
GABARAP
RIPK2
IRF7
NOS2
IL1B
RSAD2
TNFAIP3
IL1A
RNF213
ITGB1
IFNAR1
G
Log2 Fold-Change Ubiquitin
Log2 Fold-Change Protein Abundance
RIPK2
TNFAIP3
GVIN1
RNF213
GABARAP
TRIM14
CD69
IRF7
RSAD2
NOS2
IL1B
IKBKE
GVIN1
IL1RN
H
~46,000 Unique di-Gly Sites
430 CBL-Dependent Sites
I
Mtb Infected
Control vs Cbl-/-
-Log10 P-Value
Mutant Decrease
Mutant Increase
Log2 Fold-Change Ubiquitin
MERTK
ITGAX
FAF2
CBL
SLC11A2
SAMD9L
IL1B
CYP51A1
TNFRSF21
STAT5A
HERC1
ATP6V02D
3APOBEC3
ATP6V0A1
CASP1
J
Log2 Fold-Change Ubiquitin
Log2 Fold-Change Protein Abundance
IRF8
ATP6V0A1
APOBEC3
ATP6V0D2
PRKAA1
ILK
ITGAX
IL1A
FAF2
SLC11A2
SAMD9L
CYP51A1
IL1B
CBL
K
Biological Processes
Phagocytosis
Neutrophil degranulation
Iron uptake and transport
Salmonella infection
Regulation of vesicle size
Cellular response to interferon-gamma
TGF-beta receptor signaling
ROS and RNS production in phagocytes
Legionellosis
Response to oxidation stress
Vacuolar acidification
Interleukin-1 processing
Ferroptosis
Receptor internalization
Tuberculosis
Regulation of I-KB kinase/NF-KB signaling
Reactive oxygen species biosynthesis
ABC transporters in lipid homeostatis
Fold-Enrichment
-Log10 P-Value

FIGURE 4

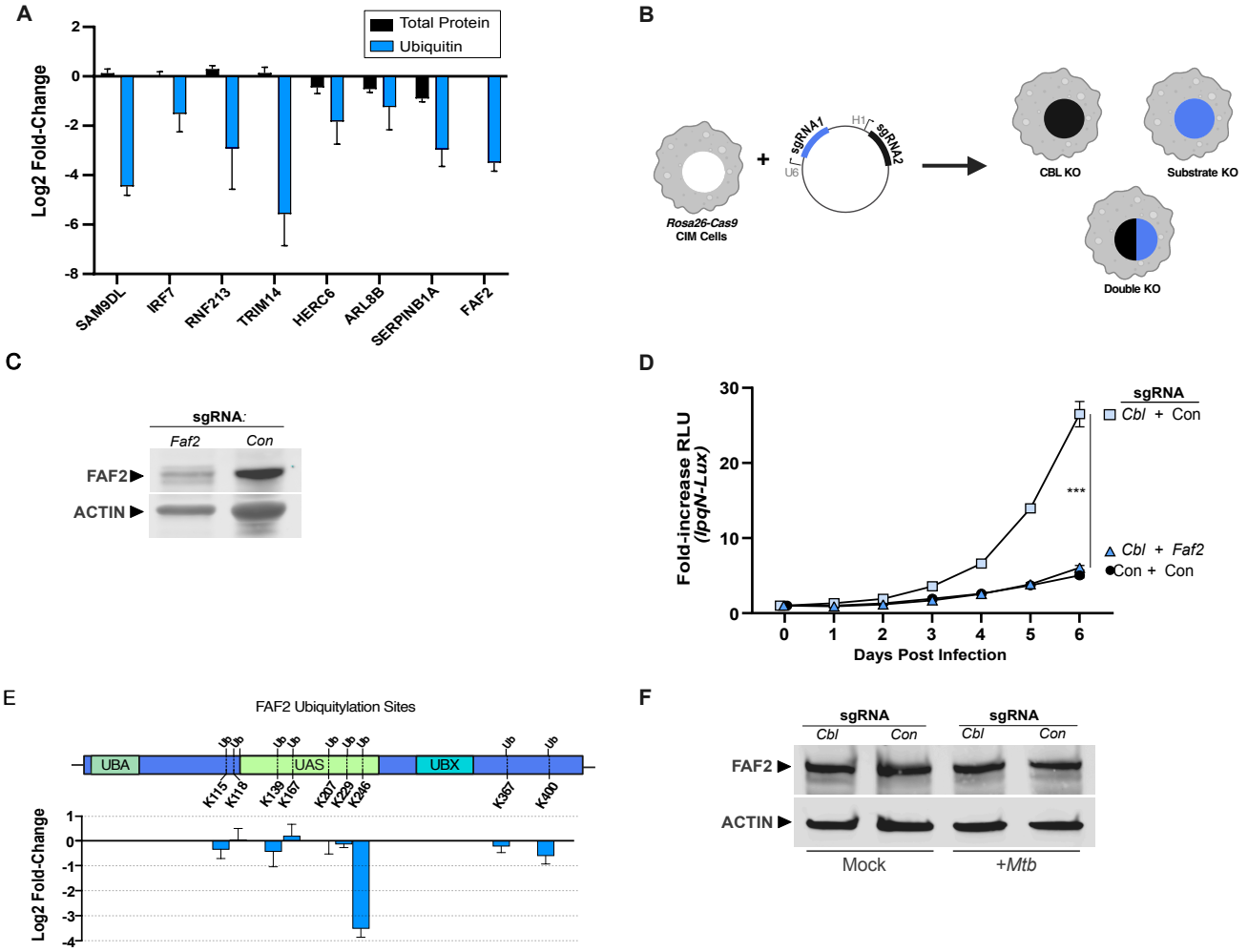
A
Total Protein
Ubiquitin
Log2 Fold-Change
2
0
-2
-4
-6
-8
SAM9DL
IRF7
RNF213
TRIM14
HERC6
ARL8B
SERPINB1A
FAF2
B
Rosa26-Cas9
CIM Cells
sgRNA1
sgRNA2
H1
U6
CBL KO
Substrate KO
Double KO
C
sgRNA:
Faf2
Con
FAF2
ACTIN
D
Fold-increase RLU
(lpqN-Lux)
30
20
10
0
sgRNA
Cbl + Con
Cbl + Faf2
Con + Con
***
0
1
2
3
4
5
6
Days Post Infection
E
FAF2 Ubiquitylation Sites
UBA
UAS
UBX
Ub
K115
K118
K139
K167
K207
K229
K246
K367
K400
Log2 Fold-Change
1
0
-1
-2
-3
-4
F
sgRNA
Cbl
Con
Cbl
Con
FAF2
ACTIN
Mock
+Mtb